Geocarto International

ISSN: (Print) (Online) Journal homepage: https://www.tandfonline.com/loi/tgei20

Examining LightGBM and CatBoost Models for Wadi Flash Flood Susceptibility Prediction

Mohamed Saber, Tayeb Boulmaiz, Mawloud Guermoui, Karim I. Abdrado, Sameh A. Kantoush, Tetsuya Sumi, Hamouda Boutaghane, Daisuke Nohara & Emad Mabrouk

To cite this article: Mohamed Saber, Tayeb Boulmaiz, Mawloud Guermoui, Karim I. Abdrado, Sameh A. Kantoush, Tetsuya Sumi, Hamouda Boutaghane, Daisuke Nohara & Emad Mabrouk (2021): Examining LightGBM and CatBoost Models for Wadi Flash Flood Susceptibility Prediction, Geocarto International, DOI: 10.1080/10106049.2021.1974959

To link to this article: https://doi.org/10.1080/10106049.2021.1974959

Accepted author version posted online: 30 Aug 2021.

Examining LightGBM and CatBoost Models for Wadi Flash Flood Susceptibility Prediction

Mohamed Saber[1,*], Tayeb Boulmaiz[2], Mawloud Guermoui[3], Karim I. Abdrado[4,5], Sameh A. Kantoush[1], Tetsuya Sumi[1], Hamouda Boutaghane[6], Daisuke Nohara[7], and Emad Mabrouk[8,9]

[1]Disaster Prevention Research Institute (DPRI), Kyoto University, Kyoto, Japan

[2]Materials, Energy Systems Technology and Environment Laboratory, Ghardaia University, Ghardaia, Algeria

[3]Unité de Recherche Appliquée en Energies Renouvelables, URAER, Centre de Développement des Energies Renouvelables, CDER, Ghardaïa, Algeria

[4]Faculty of Urban and Regional Planning, Cairo University, Giza, Egypt

[5]Department of Urban Management, Graduate School of Engineering, Kyoto University, Kyoto, Japan

[6]Hydraulic Department, Badji Mokhtar-Annaba University, Annaba, Algeria

[7]Kajima Technical Research Institute, Tokyo, Japan

[8]College of Engineering and Technology, American University of the Middle East, Egaila, Kuwait

[9]Department of Mathematics, Faculty of Science, Assiut University, Assiut, Egypt

[*]Corresponding: Mohamed Saber, mohamedmd.saber.3u@kyoto-u.ac.jp

Abstract

This study presents two machine learning models, namely, the light gradient boosting machine (LightGBM) and categorical boosting (CatBoost), for the first time for predicting flash flood susceptibility (FFS) in the Wadi System (Hurghada, Egypt). A flood inventory map with 445 flash flood sites was produced and randomly divided into two groups for training (70%) and testing (30%). Fourteen flood controlling factors were selected and evaluated for their relative importance in flood occurrence prediction. The performance of the two models was assessed using various indexes in comparison to the common random forest (RF) method. The results show areas under the receiver operating characteristic curves (AUROC) of above 97% for all models and that LightGBM outperforms other models in terms of classification metrics and processing time. The developed FFS maps demonstrate that highly populated areas are the most susceptible to flash floods. The present study proves that the employed algorithms (LightGBM and CatBoost) can be efficiently used for FFS mapping.

Keywords Machine learning algorithms, LightGBM, CatBoost, Random forest, Flash flood susceptibility mapping, Wadi System

1 Introduction

The United Nations (UNISDR 2015) stated that approximately 43% of the natural disasters that occurred globally from 1995 to 2015 and affected more than half of all people were water-related disasters. Flash floods are more catastrophic than any other type of flooding due to

their very short lag time (Vinet 2008), especially in arid environments (Negm 2020; Saber et al. 2020). The devastating impacts of flash floods have been recorded and documented in developing and developed countries (Bisht et al. 2018; Martín-Vide and Llasat 2018); however, flood events are more severe in developing countries, such as those in the Middle East and North Africa (MENA) region. The observed increase in flash flood frequency is mainly driven by changes in extreme storm patterns and global climate change (Hirabayashi et al. 2013; Pachauri et al. 2014). The frequencies of extreme flood events in the past few decades have increased in the MENA region (Zhang et al. 2005). Flash flood risk mitigation requires the use of precise and accurate flood monitoring measures to support hazard management (Arora et al. 2021). Mapping flash flood susceptibility (FFS) areas is considered one of the most important measures among scientists and governments around the world (Ali et al. 2020). This task is generally difficult and considered more difficult in the MENA region than in other regions due to difficulties with accessing affected areas; consequently, the performance of hydrological models can be affected, and detailed observational datasets are required for calibration and validation (Abushandi and Merkel 2011; Abdrabo et al. 2020).

Flood susceptibility mapping (FSM) has been conducted with several tools, such as geospatial tools available through geographic information systems (GIS) (Wang et al. 2019), the analytical hierarchy process (AHP) (Vojtek and Vojteková 2019; Abdrabo et al. 2020), the frequency ratio (FR) method (Samanta et al. 2018; Siahkamari et al. 2018) and the weights of evidence approach (Hong et al. 2018). However, these methods have drawbacks in FSM; notably, the AHP yields uncertainties associated with ambiguous judgments based on expert knowledge, which is used to set the weights of influential factors (Choubin et al. 2019), and the use of the FR is reliant on the sample size (Samanta et al. 2018; Siahkamari et al. 2018). Some additional drawbacks include predefined assumptions related to flood occurrence and the corresponding influential factors (Dodangeh et al. 2020). Moreover, many types of models, including physically based, lumped, and statistical models, have been widely used to simulate hydrological events; however, physical models present various uncertainties (Unduche et al. 2018; Chourushi et al. 2019). Such uncertainties related to reliable quantitative flood predictions are due to data limitations (Fawcett and Stone 2010; Arabameri et al. 2020), and models require the use of extensive and detailed field observations for parametrization (Fenicia et al. 2008). Therefore, alternative tools and methods for assessing FFS in ungauged basins of arid regions are needed.

Globally, the application of machine learning approaches for flood susceptibility prediction has been widely assessed over the past two decades. Therefore, the recent development of machine learning methods has led to substantial improvements in flood modeling, and such methods have become widespread due to their ability to capture information without applying predefined assumptions and to process complex datasets with high levels of accuracy in short periods of time (Costache, Popa, et al. 2020; Arabameri et al. 2020). ML models that have been used to predict flood susceptibility include logistic regression (LR), artificial neural networks (ANNs) (Arora et al. 2021; Shahabi et al. 2021), the adaptive neuro-fuzzy inference system (ANFIS) (Costache, Hong, et al. 2020; Arora et al. 2021), genetic algorithms (GAs) (Darabi et al. 2019; Shirzadi et al. 2020), support vector machines (SVMs) (Choubin et al. 2019; Dodangeh et al. 2020), and random forest (RF) models. The RF model has been widely used for flood risk assessment (Esfandiari et al. 2020; Chen et al. 2020). Additionally, various ML algorithms, together with novel ML ensemble methods, have been used to map FFS (Shahabi et al. 2021). ML approaches involve various steps (Arora et al. 2021). First, inventory datasets with reasonable accuracy must be prepared for both training and validation of the employed models. Second, the potential flood conditions or geoenvironmental factors related to flooding in the study area must be selected. Third, efficient and appropriate ML models are used, and the model performance is assessed by reliable evaluation indices.

Several studies of arid regions have been performed to develop flash flood hazard maps (Saber et al. 2020) using GIS and rainfall-runoff model (RRI) tools, to establish flood susceptibility maps using conventional methods such as AHP and ArcGIS tools as part of a

multicriteria approach (Souissi et al. 2020), and to assess flash flood hazards (Farhan and Anaba 2016; Kumar et al. 2018; Adnan et al. 2019; Abdelkader et al. 2021; Ahmed et al. 2021) using geomorphometric approaches combined with remote sensing data and rainfall-runoff modelling. Most of such studies have been limited by a lack of data available for model calibration and validation for flash flood modelling and forecasting, leading to uncertainty. Despite the challenges that have faced previous studies and attempts made to apply ML approaches to overcome such challenges, the application of ML algorithms remains limited in arid (El-Haddad et al. 2020) and semiarid regions (Janizadeh et al. 2019; Arabameri et al. 2020). Consequently, the use of ML approaches and soft computing methods is crucial and highly recommended for assessing FFS in ungauged basins of arid and semiarid regions.

In this study, we examine two methods (the light gradient boosting machine (LightGBM) and categorical boosting (CatBoost)) for FFS mapping for the first time. Both methods have been applied in other applications. For instance, LightGBM was used in previous studies due to its accurate predictions, short computational time, and outstanding ability to avoid overfitting issues. The method has been applied in the prediction of protein-protein interactions (Chen et al. 2019), price trend forecasting (Sun et al. 2020), wind power forecasting (Ju et al. 2019), flight departure delay prediction (Ye et al. 2020), web searches, miRNA identification in breast cancer (Wang et al. 2017), music recommendation challenges (Zhang and Fogelman-Soulié 2018), peer-to-peer (P2P) network credit default predictions (Ma et al. 2018), and audio scene classification systems (Gong et al. 2017). CatBoost has also been applied in many other fields, such as in driving style recognition (Liu et al. 2020) and evapotranspiration prediction in humid climate regions (Huang et al. 2019; Zhang et al. 2020). Accordingly, the main objective of this work is to evaluate how effective two machine learning approaches (LightGBM and CatBoost) are in predicting FFS in Wadi environments (the city of Hurghada and upstream Wadi catchments along the Red Sea, Egypt) and to compare the performance of these methods to that of the common RF method. The subsequent sections of this study are as follows: study area description, introduction to the datasets and methodology, presentation of the results, discussion, and conclusion.

2 Study Area

The city of Hurghada is located along the Red Sea coast, Egypt, and bounded by latitudes 270° 10′ and 270° 30′ N and longitudes 330° 30′ and 330° 52′ E, as shown in Fig. 1. The watershed area is 138 km^2, and the maximum and minimum elevations are approximately 2139 m and 13 m above sea level, respectively. The city is one of the most vulnerable areas to urban flash floods, with an increased rainfall trend from 1983 to 2019 (Abdrabo et al., 2020). Additionally, several flash flood events occurred in Hurghada and the surrounding areas, especially in the spring and autumn of 1996, 2014, 2016; these events caused severe damage to the infrastructure and other facilities of the city (ABDEL-FATTAH et al. 2015). An overall assessment of flood risk maps in Wadi Qena showed that the El-Hurghada-Ras Gharib national road is located in a basin with one of the highest hazard levels in the surrounding area (Elsadek et al. 2019). Hurghada has experienced a fast development in tourism, an immense increase in population and considerable urban growth over the past two decades; accordingly, it has become a tourist and economic hub in the region. Additionally, flash flood events in the region have become more hazardous due to increases in the flash flood frequency and intensity. The frequency and magnitude of flash floods have increased in the past two decades based on historical climatic data obtained at the Hurghada weather station (Tutiempo Network, S.L. 2021), as shown in Fig. 1c. This finding also corroborates the results of previous research on the frequency and intensity of rainfall in arid and semiarid regions (Saber et al 2020, Lu Xu et al 2020). For instance, the number of rainy days based on the Hurghada weather station data has increased (approximately 19 days) over the past decade from 2010 to 2020; however, in the previous period from 1993 to 2009, the number of rainy days was approximately 12. The exposure of lives and

infrastructure to flash floods affects social wellbeing at the individual and country levels (Fig. A.1, Appendix A).

3 Methodology

The methodology of this study consists of several steps, as illustrated in the flowchart in Fig. 2. There are two main parts in the methodology. First, a flood inventory map was developed based on the 445 flooded points. These points were identified based on field surveys and records of historical flood events. Additionally, nonflooded points (445) were randomly selected throughout the catchment using a GIS environment. Furthermore, a total of 14 independent FSS factors (FFSFs) were considered for modeling based on the local topographical, hydrological, geological and landform characteristics, which have been used in several literature studies. These FFSFs are elevation, slope, aspect, plan curvature, vertical and horizontal distance from main streams, hillshade, flow accumulation, the topographic wetness index (TWI), rainfall, lithology, land use (LU), the sediment transport index (STI), and the normalized difference vegetation index (NDVI), which were used to determine the linear relationships with other factors. In a later stage, the dataset was divided into two groups for training (70%) and testing (30%) through a random selection scheme. Spatial maps for each FFSF were produced using ArcGIS considering the consistency of the spatial resolution. Then, two methods, the information gain ratio (IGR) and multicollinearity test (VIF) methods, were used to assess the importance of FFSFs in the study area. Second, with the implementation of the proposed machine learning approaches, the datasets were divided into two main categories for training (70%) and validation (30%), and three algorithms were used: RF, LightGBM, and CatBoost. The results of the models were assessed for accuracy using different measures, including the famous area under the curve (AUC) metric.

3.1. Datasets

3.1.1. Flash flood inventory data

The first step in FFS mapping (FFSM) is to identify flood points or locations based on historical records of previous floods. Such records provide the most important inputs for FFSM (Tehrany et al. 2014). From the records of past event occurrences, locations of future hazard events can be estimated (Devkota et al. 2013). Therefore, conducting an analysis of similar past events and the corresponding influential factors is the first step in flood susceptibility assessment (Masood and Takeuchi 2012). A flood inventory map shows the sites of flooded areas in any flood-prone basin (Bellu et al. 2016). An inventory map can be prepared from several sources, including field surveys, flood forecasting records, and remote sensing data (Esfandiari et al. 2020; Band et al. 2020). Appropriately selecting flood points will enhance model accuracy for flood susceptibility prediction (Arora et al. 2019). In this study, 890 ground control points (Fig. 1a, b) were identified for both flood (445) and nonflooded points (445). The flood locations were compiled from historical flood records, inundation maps developed through rainfall-runoff modelling (Saber et al. 2020), and field surveys of flooded and affected areas (Fig. A.1, Appendix A). Nonflooded points were randomly selected. The flood and nonflooded points were assigned values of 1 and 0, respectively, and then the points were divided into sets (70% and 30%) for the training and validation of the flash flood prediction model; notably, the model's performance and generalization ability were verified based on a random selection method.

3.1.2. Geospatial database (flood-related parameters)

The selection of flood-influencing factors in FFSM is important and impacts modelling accuracy (Kia et al. 2012). During floods in drainage systems, runoff patterns are related to the characteristics of the watershed, catchment area, topography and LU/land cover types (Hölting and

Coldewey 2019). There are no standard and universal criteria for selecting the controlling factors for FSM; therefore, according to the previous review and the study area characteristics, and data availability, 14 flood-triggering factors, including topographic, hydrological, geological, and landform factors, were selected. The topographic factors are elevation, slope, plan curvature, aspect, hillshade, flow direction, and flow accumulation. The hydrological factors include the TWI, the STI, rainfall, and vertical and horizontal flow distances. The geological and land form factors include lithology, the NDVI, and LU. All data were resampled and prepared in spatial raster format with a 90-m spatial resolution in ArcGIS (Fig. 3). All topographic factors were constructed based on the Multi-Error-Removed Improved-Terrain (MERIT) DEM (Yamazaki et al. 2017). The spatial resolution of the terrain elevation is 3 sec (~90 m at the equator). This DEM was developed by eliminating the error components in existing DEMs, such as SRTM3 v2.1 and AW3D30m v1. The data are freely accessible and available at http://hydro.iis.u-tokyo.ac.jp/~yamadai/MERIT_DEM/.

3.1.2.1 Topographic factors

Elevation: There is a direct relation between elevation and flooding (Tehrany et al. 2013), which means that low land surfaces are more vulnerable to floods than high land areas (Khosravi et al. 2016); notably, the higher the elevation is, the lower the flood probability (Tehrany et al. 2014; Youssef et al. 2016). The study area has very complex topographic features, with very high elevations ranging from 500 m to more than 2000 m in the upstream zone, moderate elevations ranging from 100 m to 500 m in the middle zone, and low land areas with elevations less than 100 m in the coastal zone, which mainly includes urban and agricultural LU types (Fig. 3a).

Slope: Slope has a significant influence on flooding (Meraj et al. 2018) due to its effects on water velocity and surface runoff (Torabi Haghighi et al. 2018). Steep slopes contribute to a high water velocity and increase the flow volume in downstream areas (Chen et al. 2020). Additionally, the slope influences the hydrological features that directly affect runoff (Tehrany et al. 2019). In the study area, the slope varies from 0 to 50 degrees (Fig. 3b).

Aspect: Aspect is important for flooding (Choubin et al. 2019), as noted by Yates et al. (2002), and many hydrologic parameters are influenced by aspect. When an aspect receives low and intense sun, soil moisture will increase; consequently, the moist slope will generate runoff, contributing to flooding risks downslope (Yariyan et al. 2020). There is an indirect relationship between aspect and flooding due to the corresponding effects on several geoenvironmental factors, including soils, rainfall, and vegetation (Rahmati et al. 2016). In this study, the aspect map was categorized into 9 classes ranging from flat to northwest (Fig. 3c).

Plan curvature: Plan curvature is considered an important and essential flood-influencing factor by many researchers (Hong et al. 2018) and affects hyporheic conditions and heterogeneity (Cardenas et al. 2004). Curvature values vary between areas of accelerated runoff and those with decelerated runoff; negative and positive values are associated with increased and decreased runoff, respectively. Runoff is affected by slope shape, as flat (zero curvature) and concave (negative) forms have more potential for flooding than convex (positive) forms (Shahabi et al. 2021). For instance, concave slopes decelerate surface flows and generally increase infiltration losses (Young and Mutchler 1969), but convex slopes accelerate flow discharge, and infiltration is often limited (Cao et al., 2016). A curvature map with three main classes (concave, flat, and convex) was developed from a DEM, as shown in Fig. 3d.

Hillshade: Hillshade or toposhade is directly related to the shade and length of hillslopes, which may affect the convergence of overland flow (Aryal et al. 2003). However, the use of toposhade has been limited in previous studies (Bui et al 2019, catena), even though it was found to

be the most important factor in FFSM after slope and elevation (Bui et al. 2019); therefore, toposhade is selected as a flood-influencing factor in this study, as shown in Fig. 3e.

Flow accumulation: Flow accumulation can be estimated from flow direction parameters to show the accumulation of flows among pixels; thus, this factor is important in FSM and hydrological studies (Kazakis et al. 2015), and it has been used in some previous studies (Alipour et al. 2020). Regions with high flow accumulation have a high probability of flooding (Lehner et al. 2006). The flow accumulation map was estimated from flow direction maps using ArcGIS, as shown in Fig. 3f.

3.1.2.2 Hydrological factors

Topographic wetness index (TWI): Proposed by Beven and Kirkby (1979), the TWI expresses the water accumulation quantity per unit (or cell) in a watershed considering the downstream flow trends due to the gravitational forces (Eq. 1).

$$TWI = \ln\left(\frac{\alpha}{\tan(\beta)}\right) \quad (1)$$

where α is the cumulative upslope catchment area draining through a point (per unit contour length) and $\tan(\beta)$ represents the steepest downslope direction of a cell surface (β is the angle in degrees).

The TWI is related to the spatial changes in wetness in a catchment (Rahmati et al. 2016) and describes the location and size of saturated areas subject to overland flow (Wilson and Gallant 2000). This index quantifies the impact of the local topography on surface runoff generation (Qin et al. 2011) and reflects the long-term moisture availability in a landscape (Kopecký and Čížková 2010). The TWI varies from −7.3 to 13.28 in a given area, as demonstrated in Fig. 3g.

Sediment transport index (STI): The processes of erosion and deposition can be reflected by the STI, which was calculated using Eq. (4). The changes in a riverbed caused by these processes can lead to variations in the water storage capability of the corresponding river and may have a considerable impact on flooding. The STI was considered a flood-related influential factor (Tehrany and Jones 2017), and pixels with low STI values were associated with high flood potential. The STI in the study area varies from 0 to 1.3, as shown in Fig. 3h.

$$STI = \left(\frac{A_s}{22.13}\right)^{0.6}\left(\frac{\sin(\beta)}{0.0896}\right)^{1.3}$$

Flow distance: The distance from main rivers or streams has a considerable impact on the flooding occurrence in a given area (Glenn et al. 2012). The areas adjacent to streams are usually more prone to flooding than are other areas (Chapi et al. 2017). Additionally, the risk of flooding is proportionally related to the distance from rivers (Predick and Turner 2008), and floods frequently occur in areas adjacent to rivers (Bui et al. 2018; Darabi et al. 2019). The distance from streams signifies the distance from stream networks, which are the main conduits of overland flow (González-Arqueros et al. 2018). In this study, horizontal and vertical flow distances were estimated (Fig. 3i, j) using ArcGIS from flow accumulation, flow direction and DEM data.

Rainfall: Precipitation has a considerable effect on flooding; notably, without rainfall, flooding would not occur. The total average rainfall was estimated over the period of 2001-2019 from the Precipitation Estimation from Remotely Sensed Information using Artificial Neural Networks (PERSIANN)-Dynamic Infrared Rain Rate in Near-Real Time (PDIR-Now) dataset (Nguyen et al. 2020, p.). The data have a high global resolution (0.04° x 0.04° or = 4 km x 4 km), are

available in near-real time and are freely available and accessible for download from https://chrsdata.eng.uci.edu/. The spatial maps show that the average precipitation is highest in the downstream portion of the watershed, as shown in Fig. 3k.

3.1.2.3 Geological and landform factors

Land use and land cover: An LU and land cover layer was generated from a global cover map (Kobayashi et al 2017) developed by the geospatial information authority of Japan (Geospatial Information Authority of Japan 2021) and mainly from the Earth Resources Observation and Science (EROS) Center website (Earth Resources Observation and Science (EROS) Center 2021). LU-land cover types influence infiltration and the runoff velocity. The study area includes approximately 8 classes (Fig. 3l): urban, consolidated rock, unconsolidated sand, water bodies, sparse vegetation, shrubs, and croplands. Most of the area is covered by rocks and sand, urban areas are limited to the coast with some vegetation, and other land cover types are very rare. The accuracy of land use/landcover is very important in hydrological studies. Therefore, high resolution remote sensing data are important to enhance the urban mapping (Raju et al. 2008) and to develop classified land cover maps (Townshend et al. 1991). Such accurate maps are essential to study the effect of land use changes on hydrological regime (Sun et al. 2013; Apollonio et al. 2016).

Lithology: Lithology is an important factor due to its effects on the infiltration and the flow velocity. The lithology was developed from the geological map of Egypt 1981 (scale 1:2000000), and the source of the data is the Ministry of Industry and Mineral Resources, Egyptian Geological Survey and Mining Authority. The lithology was classified into 6 geological types (Fig. 3m), includinTable 1 g Dokhan volcanic, which is rare in the area. Carbonates are dominant in the northern part of the study area. Pleiomarine deposits are sparsely distributed throughout the area, old granite and young granites are mainly located in the upstream area, and most of the area, especially for parts of the middle and downstream regions, is dominated by Quaternary deposits. **NDVI:** NDVI data were extracted from Moderate-Resolution Imaging Spectroradiometer (MODIS) 6 data. The EROS Moderate-Resolution Imaging Spectroradiometer (eMODIS) collection was developed based on the MODIS data acquired by NASA-EOS. The spatial resolution of the data is 250 meters (m). The data can be freely accessed from the USGS at (Earth Resources Observation and Science (EROS) Center 2021). In the study area, the NDVI varies from −0.19 to 0.99 (Fig. 3n).

3.2. Selection of flood-influencing factors

Feature selection is an important step in machine learning modeling. Removing redundant features may prevent a reduction in the training process speed caused by (1) the increased number of features and (2) the loss landscape ill-conditioning issue (Öztürk and Akdeniz 2000). The latter occurs when highly correlated features exist in the training dataset, thus causing a problem in determining the learning rate hyperparameter. Therefore, an incorrect choice of this hyperparameter value may affect the model estimation ability. Therefore, the feature selection process was based on three analyses to detect irrelevant factors: (1) Spearman's rank correlation, (2) a multicollinearity test and (3) the IGR.

3.2.1. Spearman's rank correlation coefficient

Spearman's rank correlation coefficient is a nonparametric measure used to evaluate the strength of the monotonic link between two parameters X and Y. The value of the coefficient varies between −1 and 1, representing perfect negative and positive degrees of association, respectively. The closer the coefficient value is to 0, the weaker the relationship between X and Y. A Pearson correlation coefficient value larger than 0.7 is indicative of a high level of collinearity (Tien Bui et al. 2016). The correlation coefficient is calculated as follows:

$$r(x,y) = 1 - \frac{6\sum(x-y)^2}{n(n^2-1)} \qquad (3)$$

where, r is the correlation coefficient, x and y are two variables and n is the length of each variable sequence.

3.2.2. Multicollinearity test

In addition to the correlations between two features based on Spearman's coefficient, multicollinearity was assessed in this study for all influential factors considered. Multicollinearity analysis aims to detect the interrelatedness of variables and was performed (in this study) based on the VIF. This factor is commonly used in flood susceptibility assessment studies (Bui et al. 2019; Khosravi et al. 2019; Rahman et al. 2019) , and a threshold of > 5 is recommended to assess multicollinearity. However, in other cases, if the VIF value is greater than 10, the corresponding predictors are considered collinear and should excluded from modeling (Dou et al. 2019). Therefore, in this study, we used a value of 5 as the threshold for selection. The independent predictors were defined as $X = \{X_1, X_2..., X_n\}$, and R_j^2 refers to the coefficient of determination when the j^{th} independent predictor X_j is regressed for all other predictors. The VIF is calculated based on the following equation (4):

$$VIF = \frac{1}{1-R_j^2} \qquad (4)$$

3.2.3. Information gain ratio

Conditioning factors were evaluated to identify their relative importance in flood occurrence prediction using the IGR test (Quinlan 1986). This feature selection method has been considered in many classification studies (Khosravi et al. 2019). For an input with an IGR of equal to zero, no relationship exists between this factor and the output. The use of such an input in the model does not add information to the applied model and generates noise, decreasing the predictive capability of the model. Therefore, removing these factors from input sets is highly recommended. The IGR was calculated using Eq. 5:

$$IGR(x,Z) = \frac{Entropy(Z) - \sum_{i=1}^{n} \frac{|Z_i|}{|Z|} Entropy(Z_i)}{-\sum_{i=1}^{n} \frac{|Z_i|}{|Z|} log \frac{|Z_i|}{|Z|}} \qquad (5)$$

4 Machine learning methods

Supervised intelligent classifier methods can be classified into different categories. These categories include different techniques: quadratic discriminant analysis (QDA), support vector classifier (linear SVM), stochastic gradient descent, decision trees, and ANN models. Ensemble learning techniques combine multiple weak learning models to build robust learners. The aim of these predictive models is to increase the overall accuracy rate. The first type of method is based on the use of feature engineering, whereas the second type is based mainly on boosting algorithms. These boosting algorithms focus on training samples that are misclassified. Different boosting algorithms have been recently proposed for classification and regression, and the most well-known and widely used algorithms include AdaBoost (Rätsch et al. 2001), CatBoost, LightGBM, XGBoost (Chen and Guestrin 2016) and gradient boosting (Friedman 2002). In this study, we selected the RF approach, as a famous classifier algorithm, and newly applied methods for FFSM: CatBoost and LightGBM.

4.1.1. Random forests (RFs)

RFs are algorithms that have been adopted to solve many problems involving prediction and multiclassification (Schoppa et al. 2020). The RF concept was introduced by Breiman (2001) as a combination of the random subspace method and bagging ensemble learning. This classification algorithm falls in the ensemble classifier category; it is based mainly on the use of decision tree models to achieve a high classification rate. Many trees are typically generated, and a bootstrap method is used for each tree based on training data. For a given classification problem, the RF procedure involves providing each tree in the forest with input data; then, each tree individually classifies the input data into the appropriate class. Final classification is accomplished by using the majority voting scheme for all individual classifiers (trees) (Pal 2005). Decision tree classifiers have several advantages over traditional methods; notably, their results are easy to interpret, they can handle both numerical and nominal data, and they are easy to construct. Nonetheless, decision trees are not always competitive with other classification techniques (Malekipirbazari and Aksakalli 2015). The RF algorithm combines straightforward operability with a high computational speed comparable to that of ANNs and SVMs (Mosavi et al. 2018). Furthermore, RFs outperformed other techniques, including ANN, SVM, and regression models, in some previous applications in hydrology (Bachmair et al. 2017). In this study, we selected an RF as one of the most widely applicable techniques in FSM in previous studies to obtain acceptable accuracy, and the results were compared with those of the two newly developed methods.

4.1.2. Light gradient boosting machine (LightGBM)

LightGBM is a variant of the gradient boosting decision tree (GBDT) algorithm developed by Microsoft (Ke et al. 2017). The structure of this algorithm is based on weak learners that are combined to form a strong learner (Ju et al. 2019). Some changes have been made in the LightGBM model, including to the histogram, leafwise tree growth function, gradient-based one-side sampling (GOSS) and exclusive feature bundling (EFB). The time of tree construction is proportional to the split operation. Finding the best splitting point (optimal split) is an important step in most GBDT models and is based on a presorted algorithm. All sample points are scanned for each feature to estimate the information gain at all possible split points; then, the optimal segmentation point is identified. However, this process is time and memory consuming. In LightGBM, another method called the histogram-based algorithm is adopted. The objective is to group data into a histogram (bins) and choose the splitting point based on these bins (Fig. 4a). This approach considerably reduces the temporal complexity of the algorithm since the operation is based on bins instead of data.

Another difference between this model and other GBDTs is the growth of the decision tree. In LightGBM, the leafwise tree growth strategy replaces the levelwise tree growth approach. The latter can find the best possible node to split, and splitting occurs at various levels, resulting in symmetric trees (Fig. 4b). However, in LightGBM, the new strategy involves finding the leaf that will reduce the maximum error and split only that leaf without splitting others (Fig. 4b). To avoid overfitting caused by the deep growth of decision trees, a maximum leafwise depth must be set (Ge et al. 2019).

The subsampling operation is usually performed with a random sample of learning data, and a tree is constructed based on that sample. In the LightGBM model, the subsampled data are weighted. The GOSS method is based on the calculation of gradients that represent the information gain of samples. Note that data instances with small gradients indicate well-trained trees that have little impact in the training process, and data instances with large gradients are those that will

contribute more to the tree construction process. The GOSS algorithm will keep all instances with large gradients and perform random sampling for instances with small gradients. In addition to these algorithms, LightGBM uses the EFB method to reduce the dimensionality of data. EFB is a technique that bundles features that are never nonzero together into a single feature. These algorithms make LightGBM faster than other GBDT models and maintain high performance since the information is preserved to the greatest extent possible.

4.1.3. Categorical boosting (CatBoost)

The CatBoost learning algorithm is another improved GBDT approach that was proposed by Dorogush, Ershov, and Gulin (2018); it uses gradient boosting for regression trees (Friedman 2002) and builds a model in a stagewise fashion through increasingly refined approximations. In addition, several improvements to the model have been made to overcome the overfitting problem (Dorogush et al. 2018). Gradient boosting is an efficient machine learning approach that has been applied in many other fields, such as web searching, environmental variable prediction, the spatial analysis of ecological factor distributions (such as the distribution of the contaminant concentration), weather forecasting, and many others (SAFAROV et al. 2020), with acceptable results. Additionally, this approach has achieved high performance in weather forecasting (Kusiak et al. 2009), the prediction of Kickstarter campaigns (Jhaveri et al. 2019), driving style recognition (Liu et al. 2020) and diabetes prediction (Miao et al. 2019). CatBoost performs well with categorical features, but the efficiency of the model increases with the absence of categorical features. The approach used is mainly based on gradient boosting and binary tree classification. The differences between CatBoost and other boosting techniques can be summarized as follows (Hancock and Khoshgoftaar 2020).

a. An advanced algorithm is automatically integrated into the model to process categorical features as numerical data. According to Prokhorenkova et al. (2017), target statistics can be used for categorical features with minimum information loss.
b. Categorical features are fused to encompass the full advantages of features.
c. The symmetrical tree technique is applied to avoid overfitting and improve the classification accuracy.

We consider the following data sample

$$D = \{(X_j, Y_j)\}\, j = 1, \ldots, m \quad (6)$$

where, $X_j = (x_j^1, x_j^2, \ldots, x_j^n)$ is the feature vector and $Y_j \in \Re$ represents the labeled vector set (binary class). Input-output data are independently and identically distributed based on an undefined function $\rho(.)$. The main objective of the learning scheme is to train a function $H: \Re^n \to \Re$ that can reduce the expected loss Eq:$L(H) := EL(y, H(X)).L(.,.)$, the smoothing loss, is a function, and (X, Y) represents some testing data from ensemble D. The gradient boosting algorithm iteratively builds a sequence of approximations $H^t: \Re^m \to \Re$ $(t = 0, 1, 2, ...)$ in a greedy manner. The final function H^t is obtained from a previous approximation using an additive process: $H^t = H^{(t-1)} + \alpha g^t$.

$$g^t = arg\ min_{g \in G} L(H^{t-1} + g) = arg\ min_{g \in G} E\ L\big(y, H^{t-1}(X)\big) \quad (7)$$

Generally, the minimization problem is solved with a greedy approach such as the Newton method using a second-order approximation of $L(H^{t-1} + g)$ at H^{t-1} or by applying (negative) gradient steps.

4.2. Model performance validation

The receiver operating curve (ROC) is a widely used and accepted technique in geospatial analysis for determining the validity of models (Tehrany et al. 2013; Chen et al. 2020). The ROC is the most commonly applied approach for the verification of flood susceptibility and landslide models. The prediction accuracy of the examined models has been evaluated using the AUC in many previous studies (Youssef and Hegab 2019). Models that exhibit satisfactory performance generally correspond to AUC–ROC values ranging from 0.5 to 1, and a model increase can increase the AUC–ROC value. The accuracy and reliability of a model are maximized when the AUC–ROC value is equal to or close to 1.0, which reflects the capability of the model to predict disaster occurrence without bias (Bui et al. 2012).

Other statistical criteria (accuracy, precision, recall, and the F1-Score) were used to evaluate the performance of the models and to compare their robustness levels to those of other models applied in the literature. Accuracy is the ratio of accurately classified observations to the total number of observations (Eq. 8), precision is the ratio of accurately classified positive observations to the total number of classified positive observations (Eq. 9), recall (also known as sensitivity) is the ratio of accurately classified positive observations to the total number of observations (Eq. 10), and the F1-Score considers both precision and recall with a weighted average (Eq. 11).

$$Accuracy = \frac{TP+TN}{TP+TN+FP+FN} \quad (8)$$

$$Precision = \frac{TP}{TP+FP} \quad (9)$$

$$Recall = \frac{TP}{TP+FN} \quad (10)$$

$$F1-Score = 2\frac{Recall * Precision}{Recall + Precision} \quad (11)$$

where TP (true positive) denotes the number of cases correctly classified as flooded pixels, TN (true negative) denotes the number of cases correctly classified as nonflooded pixels, FP (false positive) denotes the number of cases incorrectly classified as flooded pixels, and FN (false negative) denotes the number of cases incorrectly classified as nonflooded pixels.

5 Results and discussion

5.1. Multicollinearity assessment and feature selection

The analysis of the Spearman correlation coefficients between factors (Table A.1, Appendix A) was based on a threshold greater than 0.7 according to the approach of Chen et al. (2018). Eight conditioning factors were identified as correlated: vertical distance to rivers, slope, DEM and SPI with horizontal distance to rivers, TRI, rainfall and STI, respectively. A multicollinearity analysis of the controlling factors was conducted using the VIF approach. The VIF range varied from 1.2 to 5.3, where the highest and lowest values of VIF were observed for the TRI and plan curvature, respectively (Fig. A.2a, Appendix A).

The computed IGR scores for all flood conditioning factors are illustrated in Fig. A.2b, Appendix A. All features have an IGR greater than zero, which indicates their relative importance in flood generation. Some factors, such as rainfall, TWI, DEM, and slope, have a high IGR score (greater than 0.2), and others, such as aspect, hillshade, and SPI, have low IGR scores (less than 0.05). The contribution and importance of factors based on IGR rank from high to the low as follows: vertical distance to rivers, DEM, TRI, TWI, slope, rainfall, lithology, land cover, flow accumulation, plan curvature, horizontal distance to rivers, STI, NDVI, SPI hillshade and aspect.

Based on the VIF, the factors rank as follows: TRI, SPI, vertical distance to rivers, DEM, STI, TWI, rainfall, flow accumulation, slope, horizontal distance to rivers, aspect, hillshade, NDVI, lithology, landcover, and plan curvature.

Based on the VIF values of the features, only TRI multicollinearity must be addressed because the VIF value is greater than 5; therefore, this factor was removed from the training dataset. Additionally, due to (1) the correlation between the STI and SPI and (2) the fact that the SPI value has a high VIF value (4.9), the SPI factor was removed. The other factors (vertical and horizontal distances to rivers, rainfall and the STI) were preserved despite the corresponding Spearman correlation analysis results because of their importance as reflected by their IGR scores (Fig. A.2b, Appendix A). Finally, the selected features for flood susceptibility included 14 factors: aspect, vertical and horizontal distances to rivers, hillshade, flow accumulation, slope, the DEM value, the curvature plan, the STI, the TWI, land cover, lithology, rainfall and the NDVI.

5.2. Comparison and evaluation of the models

In this section, we provide a detailed comparison of all studied models in terms of different classification metrics. The comparison was performed based on K-fold cross-validation. The studied data were partitioned into a learning set (60%) and a test set to evaluate model performance. The learning set was divided into two sets: one for training (80%) and one to update the model weights and reduce the classification errors. The validation data were used for hyperparameter selection. The optimum hyperparameters for each classification model were selected from the learning data using a grid search method. A large range of hyperparameter values was investigated. For each classifier, the best architecture is given in Table 1.

Figure 5 displays the average accuracy of the RF, CatBoost and LightGBM models. It is clear that all models provide approximately the same classification results in terms of statistical indicators, with a slight improvement for the LightGBM model in terms of speed convergence and classification metrics. Figure 6 shows the ROCs of all developed models using the test set. The simulation results demonstrate that the three selected boosting methods exhibit similar properties and provide equivalent accuracy levels. The highest AUC was obtained by the RF model (98.08%), followed by that of the LightGBM with AUC = 98.05%, and the lowest AUC was obtained by CatBoost, with AUC = 97.57%. Moreover, LightGBM displayed the most precise classification performance, with an accuracy =94.92% and precision= 95.68%, followed by the RF model, with an accuracy =94.35% and 95.14%, and finally the CatBoost model, with the same classification rate as the RF model and a 0.94% decrease in precision. In comparison with the RF models in previous studies (e.g., W. Chen et al./Science of the Total Environment 701 (2020) with AUC = 0.925, Tang et al. (2020) with AUC = 0.886, Lee et al. (2017) with AUC = 0.7878, and Achour and Pourghasemi (2020) with AUC = 0.972), the RF model in this study is superior.

In this paper, two new boosting classification techniques were investigated for FFSM in the Hurghada area. To the best of the authors' knowledge, this is the first work to investigate the use of CatBoost and LightGBM in flash flood classification problems compared to commonly used RF models. The obtained results suggest that LightGBM outperforms its counterpart models in terms of classification metrics and processing time. From the simulation results, we can conclude that LightGBM is efficient in flash flood prediction. The predictive accuracy of LightGBM (AUC = 98.5%) provides reasonable performance in flash flood prediction compared to other models. Fan et al. (2019) found that LightGBM performed better than the RF, M5Tree and other empirical models in calculating daily evapotranspiration in a humid subtropical region in China.

The accuracy of CatBoost (AUC = 97.57%) was also high compared with that reported in other studies in other fields. Notably, CatBoost, an RF and an SVM were utilized for modeling

evapotranspiration in a humid region in China (Huang et al. 2019). CatBoost yielded better accuracy and a lower computational cost than the other methods (RF and SVM).

5.3. Flash flood susceptibility modeling

The evaluation metrics of the new boosting methods (CatBoost and LightGBM) and the RF model verify the abilities and high performance of these models in the prediction of future flash floods in arid regions. Accordingly, the methods were employed to estimate the flood susceptibility in the entire study area. Three FFSMs developed based on the three methods (RF, LightGBM, and CatBoost) are shown in Fig. 7a, b, and c, respectively. The flood susceptibility values were categorized into five classes: no flooding, low, moderate, high and very high. The areas covered by the different susceptibility categories vary depending on the model. The FFSM results of the three models indicate that the areas of high and very high susceptibility to flooding cover 41% (RF), 42% (LightGBM), and 44% (CatBoost) of the study area. The areas associated with moderate and low susceptibility to flooding (Fig. 8) are estimated at 38% (RF), 34% (LightGBM), and 29% (CatBoost) of the research area. The area that is not susceptible to flash floods varies from 21% to 27% of the total study area (Fig. 8). However, the employed models perform differently in classifying the areas of various FFS levels. All methods exhibit general agreement in terms of the spatial pattern of the susceptibility classes for flooding, and coastal areas are the most prone to flooding; these areas are where most residential and agricultural regions are located in the context of the study area.

6 Discussion

Currently, increased attention is being given to data-driven methods as alternatives to traditional hydrological and hydraulic models. Therefore, the scientific community is attempting to develop new logic-based mathematical approaches to predict flood-susceptible areas at different spatial scales (Arora et al. 2021). In arid and semiarid environments, few studies have applied machine learning approaches for FFSM (El-Haddad et al. 2020). Therefore, testing different methods is highly recommended, especially in hyperarid regions where data are limited and hydrological models are challenging to establish. This study provides an assessment of three applied methods: RF, LightGBM and CatBoost. The latter two methods are newly tested for FFSM for the first time. The obtained FFS maps verify that both methods can predict flood-prone areas with acceptable accuracy in comparison with the RF method, which has been widely applied in related studies and achieved different levels of accuracy (e.g., AUC = 78% for Band et al. (2020), AUC = 99.3% for Li et al. (2019), AUC = 94.5% for Talukdar et al. (2020), AUC = 93.8% for Park and Lee (2020), and AUC = 89.4% for Nguyen et al. (2018)). In this study, the AUC = 98.2% for the RF model was higher than that in most previous studies. Additionally, the newly applied LightGBM model outperformed the RF and most previously used approaches. Additionally, the three methods showed better performance on average than previously applied methods for flood susceptibility mapping according to the approximately 140 previous applications discussed in more than 30 publications that we reviewed. The performance of the previous methods applied for FSM based on AUC varies from 64% (Shafizadeh-Moghadam et al. 2018) to 99.3% (Li et al. 2019); LightGBM yields improved classification metrics and a faster processing time. From the present results, LightGBM and CatBoost were verified as efficient in flash flood prediction in arid regions, and they can be effectively applied in other climatic regions, especially for assessments of water-related disasters such as flash floods and landslides.

7 Conclusions

Flash flood disasters are a tangible threat to society and the environment and hinder long-term sustainability, especially in arid regions where high-quality observations and flood risk management are lacking. Therefore, the present study focuses on accurately predicting FFS in a

hyperarid area of the city of Hurghada along the Red Sea. Three machine learning methods were tested to predict the FFS zones in the study area. The first method is the RF approach, which is well known and widely applied in FFM; the other two methods (LightGBM and CatBoost) are assessed for the first time for FFSM. The methods were trained and validated based on flood inventory maps and 14 flood-influencing factors considering the topographical, hydrological, geological and landform characteristics of the study area. The conclusions of this research can be summarized as follows:

1. The results of FFSM show that the applied methods can accurately predict flood zones with acceptable accuracy, with an area under the ROC above 97%.
2. The FFSM results indicate that the highly populated coastal area is more prone to flooding than other areas and is classified as highly and very highly susceptible.
3. The study verified that the newly applied ML algorithms (LightGBM and CatBoost) can potentially be used for FFSM.
4. The outcomes of this study can be used as a reference to guide flash flood risk management and mitigation in arid regions and consequently assist planners and managers in mitigating flash floods in highly flood-susceptible regions.

Acknowledgments

LU/land cover data were provided by the Geospatial Information Authority of Japan, Chiba University and collaborating organizations. We thank Eng. Ibrahim Mohamed Abdou, PhD Student of the Faculty of Urban and Regional Planning at Cairo University, for his support in collecting data on flood occurrence in Hurghada for recent flash floods. This paper was funded by

Funding

This work was supported by the JSPS Fund for the Promotion of Joint International Research (Fostering Joint International Research (B)); No. 20KK0094) and Innovative Africa: Educational Networking Programs for Human Resource Development in Africa's SDGs, an interuniversity exchange program Kyoto University received from the Japanese Ministry of Education, Culture, Sports, Science and Technology (MEXT).

Declaration of Competing Interests

The authors declare that they have no known competing financial interests or personal relationships that could have appeared to influence the work reported in this paper.

Data availability statement

The data that support the findings of this study are available from the corresponding author upon reasonable request.

8 References

ABDEL-FATTAH M, KANTOUSH S, SUMI T. 2015. Integrated management of flash flood in wadi system of egypt: Disaster prevention and water harvesting.

Abdel-Fattah M, Kantoush SA, Saber M, Sumi T. 2018. Rainfall-runoff modeling for extreme flash floods in wadi samail, oman. Journal of Japan Society of Civil Engineers, Ser B1 (Hydraulic Engineering). 74(5):I_691-I_696.

Abdelkader MM, Al-Amoud AI, El Alfy M, El-Feky A, Saber M. 2021. Assessment of flash flood hazard based on morphometric aspects and rainfall-runoff modeling in Wadi Nisah, Central Saudi Arabia. Remote Sensing Applications: Society and Environment.:100562.

Abdrabo KI, Kantoush SA, Saber M, Sumi T, Habiba OM, Elleithy D, Elboshy B. 2020. Integrated Methodology for Urban Flood Risk Mapping at the Microscale in Ungauged Regions: A Case Study of Hurghada, Egypt. Remote Sensing. 12(21):3548. https://doi.org/10.3390/rs12213548

Abdulwahab Aboualnaga. 2014. The Zafarana-Hurghada road was closed due to the floods. Mobtda [Internet]. https://www.mobtada.com/details/186604

Abushandi EH, Merkel BJ. 2011. Application of IHACRES rainfall-runoff model to the Wadi Dhuliel arid catchment, Jordan. Journal of Water and Climate Change. 2(1):56–71.

Achour Y, Pourghasemi HR. 2020. How do machine learning techniques help in increasing accuracy of landslide susceptibility maps? Geoscience Frontiers. 11(3):871–883.

Adnan MSG, Dewan A, Zannat KE, Abdullah AYM. 2019. The use of watershed geomorphic data in flash flood susceptibility zoning: a case study of the Karnaphuli and Sangu river basins of Bangladesh. Natural Hazards. 99(1):425–448.

Ahmed A, Hewa G, Alrajhi A. 2021. Flood susceptibility mapping using a geomorphometric approach in South Australian basins. Natural Hazards. 106(1):629–653.

Al-Abadi AM. 2018. Mapping flood susceptibility in an arid region of southern Iraq using ensemble machine learning classifiers: a comparative study. Arab J Geosci. 11(9):218. https://doi.org/10.1007/s12517-018-3584-5

Ali SA, Parvin F, Pham QB, Vojtek M, Vojteková J, Costache R, Linh NTT, Nguyen HQ, Ahmad A, Ghorbani MA. 2020. GIS-based comparative assessment of flood susceptibility mapping using hybrid multi-criteria decision-making approach, naïve Bayes tree, bivariate statistics and logistic regression: A case of Topľa basin, Slovakia. Ecological Indicators. 117:106620.

Alipour A, Ahmadalipour A, Abbaszadeh P, Moradkhani H. 2020. Leveraging machine learning for predicting flash flood damage in the Southeast US. Environ Res Lett. 15(2):024011. https://doi.org/10.1088/1748-9326/ab6edd

Apollonio C, Balacco G, Novelli A, Tarantino E, Piccinni AF. 2016. Land use change impact on flooding areas: The case study of Cervaro Basin (Italy). Sustainability. 8(10):996.

Arabameri A, Saha S, Mukherjee K, Blaschke T, Chen W, Ngo PTT, Band SS. 2020. Modeling Spatial Flood using Novel Ensemble Artificial Intelligence Approaches in Northern Iran. Remote Sensing. 12(20):3423. https://doi.org/10.3390/rs12203423

Arora A, Arabameri A, Pandey M, Siddiqui MA, Shukla UK, Bui DT, Mishra VN, Bhardwaj A. 2020. Optimization of state-of-the-art fuzzy-metaheuristic ANFIS-based machine learning models for flood susceptibility prediction mapping in the Middle Ganga Plain, India. Science of The Total Environment. 750:141565. https://doi.org/10.1016/j.scitotenv.2020.141565

Arora A, Pandey M, Siddiqui MA, Hong H, Mishra VN. 2019. Spatial flood susceptibility prediction in Middle Ganga Plain: comparison of frequency ratio and Shannon's entropy models. Geocarto International.:1–32.

Aryal SK, Mein RG, O'Loughlin EM. 2003. The concept of effective length in hillslopes: assessing the influence of climate and topography on the contributing areas of catchments. Hydrological processes. 17(1):131–151.

Bachmair S, Svensson C, Prosdocimi I, Hannaford J, Stahl K. 2017. Developing drought impact functions for drought risk management. Natural Hazards and Earth System Sciences. 17(11):1947–1960.

Band SS, Janizadeh S, Chandra Pal S, Saha A, Chakrabortty R, Melesse AM, Mosavi A. 2020. Flash Flood Susceptibility Modeling Using New Approaches of Hybrid and Ensemble Tree-Based Machine Learning Algorithms. Remote Sensing. 12(21):3568. https://doi.org/10.3390/rs12213568

Bellu A, Fernandes LFS, Cortes RM, Pacheco FA. 2016. A framework model for the dimensioning and allocation of a detention basin system: The case of a flood-prone mountainous watershed. Journal of Hydrology. 533:567–580.

Beven KJ, Kirkby MJ. 1979. A physically based, variable contributing area model of basin hydrology/Un modèle à base physique de zone d'appel variable de l'hydrologie du bassin versant. Hydrological Sciences Journal. 24(1):43–69.

Bisht S, Chaudhry S, Sharma S, Soni S. 2018. Assessment of flash flood vulnerability zonation through Geospatial technique in high altitude Himalayan watershed, Himachal Pradesh India. Remote Sensing Applications: Society and Environment. 12:35–47.

Breiman L. 2001. Random forests. Machine learning. 45(1):5–32.

Bui DT, Hoang N-D, Pham T-D, Ngo P-TT, Hoa PV, Minh NQ, Tran X-T, Samui P. 2019. A new intelligence approach based on GIS-based multivariate adaptive regression splines and metaheuristic optimization for predicting flash flood susceptible areas at high-frequency tropical typhoon area. Journal of Hydrology. 575:314–326.

Bui DT, Panahi M, Shahabi H, Singh VP, Shirzadi A, Chapi K, Khosravi K, Chen W, Panahi S, Li S. 2018. Novel hybrid evolutionary algorithms for spatial prediction of floods. Scientific reports. 8(1):1–14.

Bui DT, Pradhan B, Lofman O, Revhaug I, Dick OB. 2012. Spatial prediction of landslide hazards in Hoa Binh province (Vietnam): a comparative assessment of the efficacy of evidential belief functions and fuzzy logic models. Catena. 96:28–40.

Cardenas MB, Wilson J, Zlotnik VA. 2004. Impact of heterogeneity, bed forms, and stream curvature on subchannel hyporheic exchange. Water Resources Research. 40(8).

Chapi K, Singh VP, Shirzadi A, Shahabi H, Bui DT, Pham BT, Khosravi K. 2017. A novel hybrid artificial intelligence approach for flood susceptibility assessment. Environmental modelling & software. 95:229–245.

Chen C, Zhang Q, Ma Q, Yu B. 2019. LightGBM-PPI: Predicting protein-protein interactions through LightGBM with multi-information fusion. Chemometrics and Intelligent Laboratory Systems. 191:54–64.

Chen T, Guestrin C. 2016. Xgboost: A scalable tree boosting system. In: [place unknown]; p. 785–794.

Chen T-HK, Qiu C, Schmitt M, Zhu XX, Sabel CE, Prishchepov AV. 2020. Mapping horizontal and vertical urban densification in Denmark with Landsat time-series from 1985 to 2018: A semantic segmentation solution. Remote Sensing of Environment. 251:112096. https://doi.org/10.1016/j.rse.2020.112096

Choubin B, Moradi E, Golshan M, Adamowski J, Sajedi-Hosseini F, Mosavi A. 2019. An ensemble prediction of flood susceptibility using multivariate discriminant analysis, classification and regression trees, and support vector machines. Science of the Total Environment. 651:2087–2096.

Chourushi S, Lodha P, Prakash I. 2019. A Critical Review of Hydrological Modeling Practices for Flood Management. Pramana Res J. 9:352–362.

Costache R, Hong H, Pham QB. 2020. Comparative assessment of the flash-flood potential within small mountain catchments using bivariate statistics and their novel hybrid integration with machine learning models. Science of The Total Environment. 711:134514. https://doi.org/10.1016/j.scitotenv.2019.134514

Costache R, Popa MC, Tien Bui D, Diaconu DC, Ciubotaru N, Minea G, Pham QB. 2020. Spatial predicting of flood potential areas using novel hybridizations of fuzzy decision-making, bivariate statistics, and machine learning. Journal of Hydrology. 585:124808. https://doi.org/10.1016/j.jhydrol.2020.124808

Courtesy Abdelhameed. 2016. In pictures: Heavy rains hit Egypt's Red Sea governorate. Al Arabiya News [Internet]. https://english.alarabiya.net/News/middle-east/2016/10/27/In-pictures-Heavy-rains-hit-Egypt-s-Red-Sea-governorate

Darabi H, Choubin B, Rahmati O, Haghighi AT, Pradhan B, Kløve B. 2019. Urban flood risk mapping using the GARP and QUEST models: A comparative study of machine learning techniques. Journal of hydrology. 569:142–154.

Devkota KC, Regmi AD, Pourghasemi HR, Yoshida K, Pradhan B, Ryu IC, Dhital MR, Althuwaynee OF. 2013. Landslide susceptibility mapping using certainty factor, index of entropy and logistic regression models in GIS and their comparison at Mugling–Narayanghat road section in Nepal Himalaya. Natural hazards. 65(1):135–165.

Dodangeh E, Choubin B, Eigdir AN, Nabipour N, Panahi M, Shamshirband S, Mosavi A. 2020. Integrated machine learning methods with resampling algorithms for flood susceptibility prediction. Science of The Total Environment. 705:135983. https://doi.org/10.1016/j.scitotenv.2019.135983

Dorogush AV, Ershov V, Gulin A. 2018. CatBoost: gradient boosting with categorical features support. arXiv preprint arXiv:181011363.

Dou J, Yunus AP, Bui DT, Merghadi A, Sahana M, Zhu Z, Chen C-W, Khosravi K, Yang Y, Pham BT. 2019. Assessment of advanced random forest and decision tree algorithms for modeling rainfall-induced landslide susceptibility in the Izu-Oshima Volcanic Island, Japan. Science of the total environment. 662:332–346.

Earth Resources Observation and Science (EROS) Center. 2021. USGS EROS Archive - Vegetation Monitoring - EROS Moderate Resolution Imaging Spectroradiometer (eMODIS). USGS [Internet]. https://www.usgs.gov/centers/eros/science/usgs-eros-archive-vegetation-monitoring-eros-moderate-resolution-imaging?qt-science_center_objects=0#qt-science

El-Haddad BA, Youssef AM, Pourghasemi HR, Pradhan B, El-Shater A-H, El-Khashab MH. 2020. Flood susceptibility prediction using four machine learning techniques and comparison of their performance at Wadi Qena Basin, Egypt. Nat Hazards [Internet]. [accessed 2020 Dec 11]. https://doi.org/10.1007/s11069-020-04296-y

Elsadek WM, Ibrahim MG, Mahmod WE, Kanae S. 2019. Developing an overall assessment map for flood hazard on large area watershed using multi-method approach: case study of Wadi Qena watershed, Egypt. Natural Hazards. 95(3):739–767.

Erdal HI, Karakurt O. 2013. Advancing monthly streamflow prediction accuracy of CART models using ensemble learning paradigms. Journal of Hydrology. 477:119–128.

Esfandiari M, Jabari S, McGrath H, Coleman D. 2020. FLOOD MAPPING USING RANDOM FOREST AND IDENTIFYING THE ESSENTIAL CONDITIONING FACTORS; A CASE STUDY IN FREDERICTON, NEW BRUNSWICK, CANADA. ISPRS Annals of Photogrammetry, Remote Sensing & Spatial Information Sciences. 5(3).

Farhan Y, Anaba O. 2016. Flash flood risk estimation of Wadi Yutum (Southern Jordan) watershed using GIS based morphometric analysis and remote sensing techniques. Open Journal of Modern Hydrology. 6(02):79.

Fawcett R, Stone R. 2010. A comparison of two seasonal rainfall forecasting systems for Australia. Australian Meteorological and Oceanographic Journal. 60(1):15–24.

Fenicia F, Savenije HH, Matgen P, Pfister L. 2008. Understanding catchment behavior through stepwise model concept improvement. Water Resources Research. 44(1).

Friedman JH. 2002. Stochastic gradient boosting. Computational statistics & data analysis. 38(4):367–378.

Ge X, Sun J, Lu B, Chen Q, Xun W, Jin Y. 2019. Classification of oolong tea varieties based on hyperspectral imaging technology and BOSS-LightGBM model. Journal of Food Process Engineering. 42(8):e13289.

Geospatial Information Authority of Japan. 2021. Global Map Global version. Geospatial Information Authority of Japan [Internet]. https://www.gsi.go.jp/kankyochiri/gm_global_e.html

Gigović L, Pamučar D, Bajić Z, Drobnjak S. 2017. Application of GIS-interval rough AHP methodology for flood hazard mapping in urban areas. Water. 9(6):360.

Glenn EP, Morino K, Nagler PL, Murray RS, Pearlstein S, Hultine KR. 2012. Roles of saltcedar (Tamarix spp.) and capillary rise in salinizing a non-flooding terrace on a flow-regulated desert river. Journal of arid environments. 79:56–65.

Gong R, Fonseca E, Bogdanov D, Slizovskaia O, Gomez E, Serra X. 2017. Acoustic scene classification by fusing LightGBM and VGG-net multichannel predictions. In: [place unknown]; p. 1–4.

González-Arqueros ML, Mendoza ME, Bocco G, Castillo BS. 2018. Flood susceptibility in rural settlements in remote zones: The case of a mountainous basin in the Sierra-Costa region of Michoacán, Mexico. Journal of environmental management. 223:685–693.

Hancock JT, Khoshgoftaar TM. 2020. CatBoost for big data: an interdisciplinary review. Journal of big Data. 7(1):1–45.

Hirabayashi Y, Mahendran R, Koirala S, Konoshima L, Yamazaki D, Watanabe S, Kim H, Kanae S. 2013. Global flood risk under climate change. Nature Climate Change. 3(9):816–821.

Hölting B, Coldewey WG. 2019. Surface water infiltration. In: Hydrogeology. [place unknown]: Springer; p. 33–37.

Hong H, Tsangaratos P, Ilia I, Liu J, Zhu A-X, Chen W. 2018. Application of fuzzy weight of evidence and data mining techniques in construction of flood susceptibility map of Poyang County, China. Science of the total environment. 625:575–588.

Hosseini FS, Choubin B, Mosavi A, Nabipour N, Shamshirband S, Darabi H, Haghighi AT. 2020. Flash-flood hazard assessment using ensembles and Bayesian-based machine learning models: Application of the simulated annealing feature selection method. Science of The Total Environment. 711:135161. https://doi.org/10.1016/j.scitotenv.2019.135161

Huang G, Wu L, Ma X, Zhang W, Fan J, Yu X, Zeng W, Zhou H. 2019. Evaluation of CatBoost method for prediction of reference evapotranspiration in humid regions. Journal of Hydrology. 574:1029–1041.

Janizadeh S, Avand M, Jaafari A, Phong TV, Bayat M, Ahmadisharaf E, Prakash I, Pham BT, Lee S. 2019. Prediction Success of Machine Learning Methods for Flash Flood Susceptibility Mapping in the Tafresh Watershed, Iran. Sustainability. 11(19):5426. https://doi.org/10.3390/su11195426

Jhaveri S, Khedkar I, Kantharia Y, Jaswal S. 2019. Success prediction using random forest, catboost, xgboost and adaboost for kickstarter campaigns. In: [place unknown]: IEEE; p. 1170–1173.

Jihad Alansary. 2014. Hurghada road collapse due to floods. Misr News [Internet]. https://masralarabia.net/%D8%A7%D8%AE%D8%A8%D8%A7%D8%B1-%D9%85%D8%B5%D8%B1/230487-%D9%81%D9%8A%D8%AF%D9%8A%D9%88-%D8%A7%D9%86%D9%87%D9%8A%D8%A7%D8%B1-%D8%A8%D8%B7%D8%B1%D9%8A%D9%82-%D8%A7%D9%84%D8%BA%D8%B1%D8%AF%D9%82%D8%A9-%D8%A8%D8%B3%D8%A8%D8%A8-%D8%A7%D9%84%D8%B3%D9%8A%D9%88%D9%84

Ju Y, Sun G, Chen Q, Zhang M, Zhu H, Rehman MU. 2019. A model combining convolutional neural network and LightGBM algorithm for ultra-short-term wind power forecasting. IEEE Access. 7:28309–28318.

Kazakis N, Kougias I, Patsialis T. 2015. Assessment of flood hazard areas at a regional scale using an index-based approach and Analytical Hierarchy Process: Application in Rhodope–Evros region, Greece. Science of the Total Environment. 538:555–563.

Ke G, Meng Q, Finley T, Wang T, Chen W, Ma W, Ye Q, Liu T-Y. 2017. Lightgbm: A highly efficient gradient boosting decision tree. Advances in neural information processing systems. 30:3146–3154.

Khosravi K, Nohani E, Maroufinia E, Pourghasemi HR. 2016. A GIS-based flood susceptibility assessment and its mapping in Iran: a comparison between frequency ratio and weights-of-evidence bivariate statistical models with multi-criteria decision-making technique. Natural Hazards. 83(2):947–987.

Khosravi K, Shahabi H, Pham BT, Adamowski J, Shirzadi A, Pradhan B, Dou J, Ly H-B, Gróf G, Ho HL, et al. 2019. A comparative assessment of flood susceptibility modeling using Multi-Criteria Decision-Making Analysis and Machine Learning Methods. Journal of Hydrology. 573:311–323. https://doi.org/10.1016/j.jhydrol.2019.03.073

Kia MB, Pirasteh S, Pradhan B, Mahmud AR, Sulaiman WNA, Moradi A. 2012. An artificial neural network model for flood simulation using GIS: Johor River Basin, Malaysia. Environmental Earth Sciences. 67(1):251–264.

Kopecký M, Čížková Š. 2010. Using topographic wetness index in vegetation ecology: does the algorithm matter? Applied Vegetation Science. 13(4):450–459.

Kumar R, Singh R, Gautam H, Pandey MK. 2018. Flood hazard assessment of August 20, 2016 floods in Satna district, Madhya Pradesh, India. Remote Sensing Applications: Society and Environment. 11:104–118.

Kusiak A, Zheng H, Song Z. 2009. Models for monitoring wind farm power. Renewable Energy. 34(3):583–590.

Lee Sunmin, Kim J-C, Jung H-S, Lee MJ, Lee Saro. 2017. Spatial prediction of flood susceptibility using random-forest and boosted-tree models in Seoul metropolitan city, Korea. Geomatics, Natural Hazards and Risk. 8(2):1185–1203.

Lehner B, Döll P, Alcamo J, Henrichs T, Kaspar F. 2006. Estimating the impact of global change on flood and drought risks in Europe: a continental, integrated analysis. Climatic Change. 75(3):273–299.

Li X, Yan D, Wang K, Weng B, Qin T, Liu S. 2019. Flood Risk Assessment of Global Watersheds Based on Multiple Machine Learning Models. Water. 11(8):1654. https://doi.org/10.3390/w11081654

Liu W, Deng K, Zhang X, Cheng Y, Zheng Z, Jiang F, Peng J. 2020. A semi-supervised tri-catboost method for driving style recognition. Symmetry. 12(3):336.

Ma X, Sha J, Wang D, Yu Y, Yang Q, Niu X. 2018. Study on a prediction of P2P network loan default based on the machine learning LightGBM and XGboost algorithms according to different high dimensional data cleaning. Electronic Commerce Research and Applications. 31:24–39.

Malekipirbazari M, Aksakalli V. 2015. Risk assessment in social lending via random forests. Expert Systems with Applications. 42(10):4621–4631.

Martín-Vide JP, Llasat M. 2018. The 1962 flash flood in the Rubí stream (Barcelona, Spain). Journal of hydrology. 566:441–454.

Masood M, Takeuchi K. 2012. Assessment of flood hazard, vulnerability and risk of mid-eastern Dhaka using DEM and 1D hydrodynamic model. Natural hazards. 61(2):757–770.

Meraj G, Khan T, Romshoo SA, Farooq M, Rohitashw K, Sheikh BA. 2018. An integrated geoinformatics and hydrological modelling-based approach for effective flood management in the Jhelum Basin, NW Himalaya. Multidisciplinary Digital Publishing Institute Proceedings. 7(1):8.

Miao H, Zhang J, Gu B, Gao A, Hong J, Zhang Y, Gu W. 2019. Prognosis for residual islet β-cell secretion function in young patients with newly diagnosed type 1 diabetes. Journal of diabetes. 11(10):818–825.

Mohamed Soliman. 2015. Rain fell in Hurghada ... and the emergency was raised in anticipation of its turning into floods. Al masry Elyoum [Internet]. https://www.almasryalyoum.com/news/details/830677

Mosavi A, Ozturk P, Chau K. 2018. Flood prediction using machine learning models: Literature review. Water. 10(11):1536.

Negm AM, editor. 2020. Flash Floods in Egypt [Internet]. Cham: Springer International Publishing; [accessed 2020 Oct 21]. https://doi.org/10.1007/978-3-030-29635-3

Nguyen P, Ombadi M, Gorooh VA, Shearer EJ, Sadeghi M, Sorooshian S, Hsu K, Bolvin D, Ralph MF. 2020. PERSIANN Dynamic Infrared–Rain Rate (PDIR-Now): A Near-Real-Time, Quasi-Global Satellite Precipitation Dataset. Journal of Hydrometeorology. 21(12):2893–2906.

Nguyen V-N, Tien Bui D, Ngo P-TT, Nguyen Q-P, Nguyen VC, Long NQ, Revhaug I. 2018. An Integration of Least Squares Support Vector Machines and Firefly Optimization Algorithm for Flood Susceptible Modeling Using GIS. In: Tien Bui D, Ngoc Do A, Bui H-B, Hoang N-D, editors. Advances and Applications in Geospatial Technology and Earth Resources [Internet]. Cham: Springer International Publishing; [accessed 2020 Dec 11]; p. 52–64. https://doi.org/10.1007/978-3-319-68240-2_4

Öztürk F, Akdeniz F. 2000. Ill-conditioning and multicollinearity. Linear Algebra and Its Applications. 321(1–3):295–305.

Pachauri RK, Allen MR, Barros VR, Broome J, Cramer W, Christ R, Church JA, Clarke L, Dahe Q, Dasgupta P. 2014. Climate change 2014: synthesis report. Contribution of Working Groups I, II and III to the fifth assessment report of the Intergovernmental Panel on Climate Change. [place unknown]: Ipcc.

Pal M. 2005. Random forest classifier for remote sensing classification. International journal of remote sensing. 26(1):217–222.

Park S-J, Lee D-K. 2020. Prediction of coastal flooding risk under climate change impacts in South Korea using machine learning algorithms. Environ Res Lett. 15(9):094052. https://doi.org/10.1088/1748-9326/aba5b3

Predick KI, Turner MG. 2008. Landscape configuration and flood frequency influence invasive shrubs in floodplain forests of the Wisconsin River (USA). Journal of Ecology. 96(1):91–102.

Prokhorenkova L, Gusev G, Vorobev A, Dorogush AV, Gulin A. 2017. CatBoost: unbiased boosting with categorical features. arXiv preprint arXiv:170609516.

Qin C-Z, Zhu A-X, Pei T, Li B-L, Scholten T, Behrens T, Zhou C-H. 2011. An approach to computing topographic wetness index based on maximum downslope gradient. Precision agriculture. 12(1):32–43.

Quinlan JR. 1986. Induction of decision trees. Machine learning. 1(1):81–106.

Rahman M, Ningsheng C, Islam MM, Dewan A, Iqbal J, Washakh RMA, Shufeng T. 2019. Flood susceptibility assessment in Bangladesh using machine learning and multi-criteria decision analysis. Earth Systems and Environment. 3(3):585–601.

Rahmati O, Pourghasemi HR, Zeinivand H. 2016. Flood susceptibility mapping using frequency ratio and weights-of-evidence models in the Golastan Province, Iran. Geocarto International. 31(1):42–70.

Raju KP, Kumar S, Mohan K, Pandey MK. 2008. Urban cadastral mapping using very high resolution remote sensing data. Journal of the Indian Society of Remote Sensing. 36(3):283–288.

Rätsch G, Onoda T, Müller K-R. 2001. Soft margins for AdaBoost. Machine learning. 42(3):287–320.

Saber M, Abdrabo KI, Habiba OM, Kantosh SA, Sumi T. 2020. Impacts of Triple Factors on Flash Flood Vulnerability in Egypt: Urban Growth, Extreme Climate, and Mismanagement. Geosciences. 10(1):24.

SAFAROV RZ, SHOMANOVA ZK, NOSSENKO YG, BERDENOV ZG, BEXEITOVA ZB, SHOMANOV AS, MANSUROVA M. 2020. Solving of Classification Problem in Spatial Analysis Applying the Technology of Gradient Boosting Catboost. Folia Geographica. 62(1):112–126.

Samanta S, Pal DK, Palsamanta B. 2018. Flood susceptibility analysis through remote sensing, GIS and frequency ratio model. Applied Water Science. 8(2):1–14.

Schoppa L, Disse M, Bachmair S. 2020. Evaluating the performance of random forest for large-scale flood discharge simulation. Journal of Hydrology. 590:125531.

Shafizadeh-Moghadam H, Valavi R, Shahabi H, Chapi K, Shirzadi A. 2018. Novel forecasting approaches using combination of machine learning and statistical models for flood susceptibility mapping. Journal of Environmental Management. 217:1–11. https://doi.org/10.1016/j.jenvman.2018.03.089

Shahabi H, Shirzadi A, Ronoud S, Asadi S, Pham BT, Mansouripour F, Geertsema M, Clague JJ, Bui DT. 2020. Flash flood susceptibility mapping using a novel deep learning model based on deep belief network, back propagation and genetic algorithm. Geoscience Frontiers.:S1674987120302401. https://doi.org/10.1016/j.gsf.2020.10.007

Shirzadi A, Asadi S, Shahabi H, Ronoud S, Clague JJ, Khosravi K, Pham BT, Ahmad BB, Bui DT. 2020. A novel ensemble learning based on Bayesian Belief Network coupled with an extreme learning machine for flash flood susceptibility mapping. Engineering Applications of Artificial Intelligence. 96:103971.

Siahkamari S, Haghizadeh A, Zeinivand H, Tahmasebipour N, Rahmati O. 2018. Spatial prediction of flood-susceptible areas using frequency ratio and maximum entropy models. Geocarto international. 33(9):927–941.

Souissi D, Zouhri L, Hammami S, Msaddek MH, Zghibi A, Dlala M. 2020. GIS-based MCDM–AHP modeling for flood susceptibility mapping of arid areas, southeastern Tunisia. Geocarto International. 35(9):991–1017.

Sun X, Liu M, Sima Z. 2020. A novel cryptocurrency price trend forecasting model based on LightGBM. Finance Research Letters. 32:101084.

Sun Z, Li X, Fu W, Li Y, Tang D. 2013. Long-term effects of land use/land cover change on surface runoff in urban areas of Beijing, China. Journal of Applied Remote Sensing. 8(1):084596.

Talukdar S, Ghose B, Salam R, Mahato S, Pham QB, Linh NTT, Costache R, Avand M. 2020. Flood susceptibility modeling in Teesta River basin, Bangladesh using novel ensembles of bagging algorithms. Stochastic Environmental Research and Risk Assessment. 34(12):2277–2300.

Tang X, Li J, Liu M, Liu W, Hong H. 2020. Flood susceptibility assessment based on a novel random Naïve Bayes method: A comparison between different factor discretization methods. Catena. 190:104536.

Tehrany M, Jones S. 2017. Evaluating the variations in the flood susceptibility maps accuracies due to the alterations in the type and extent of the flood inventory. In: Vol. 42. [place unknown]; p. 4.

Tehrany MS, Jones S, Shabani F. 2019. Identifying the essential flood conditioning factors for flood prone area mapping using machine learning techniques. CATENA. 175:174–192. https://doi.org/10.1016/j.catena.2018.12.011

Tehrany MS, Kumar L. 2018. The application of a Dempster–Shafer-based evidential belief function in flood susceptibility mapping and comparison with frequency ratio and logistic regression methods. Environmental Earth Sciences. 77(13):1–24.

Tehrany MS, Pradhan B, Jebur MN. 2013. Spatial prediction of flood susceptible areas using rule based decision tree (DT) and a novel ensemble bivariate and multivariate statistical models in GIS. Journal of Hydrology. 504:69–79.

Tehrany MS, Pradhan B, Jebur MN. 2014. Flood susceptibility mapping using a novel ensemble weights-of-evidence and support vector machine models in GIS. Journal of hydrology. 512:332–343.

Tehrany MS, Pradhan B, Jebur MN. 2015. Flood susceptibility analysis and its verification using a novel ensemble support vector machine and frequency ratio method. Stochastic environmental research and risk assessment. 29(4):1149–1165.

Tien Bui D, Pradhan B, Nampak H, Bui Q-T, Tran Q-A, Nguyen Q-P. 2016. Hybrid artificial intelligence approach based on neural fuzzy inference model and metaheuristic optimization for flood susceptibilitgy modeling in a high-frequency tropical cyclone area using GIS. Journal of Hydrology. 540:317–330. https://doi.org/10.1016/j.jhydrol.2016.06.027

Torabi Haghighi A, Menberu MW, Darabi H, Akanegbu J, Kløve B. 2018. Use of remote sensing to analyse peatland changes after drainage for peat extraction. Land Degradation & Development. 29(10):3479–3488.

Townshend J, Justice C, Li W, Gurney C, McManus J. 1991. Global land cover classification by remote sensing: present capabilities and future possibilities. Remote Sensing of Environment. 35(2–3):243–255.

Tutiempo Network, S.L. 2021. Climate Hurguada. Tutiempo Network, SL [Internet]. [accessed 2021 Mar 3]. https://en.tutiempo.net/climate/ws-624630.html

Unduche F, Tolossa H, Senbeta D, Zhu E. 2018. Evaluation of four hydrological models for operational flood forecasting in a Canadian Prairie watershed. Hydrological Sciences Journal. 63(8):1133–1149.

UNISDR C. 2015. The human cost of natural disasters: A global perspective [Internet]. [place unknown]. https://reliefweb.int/sites/reliefweb.int/files/resources/PAND_report.pdf

Vinet F. 2008. Geographical analysis of damage due to flash floods in southern France: The cases of 12–13 November 1999 and 8–9 September 2002. Applied Geography. 28(4):323–336. https://doi.org/10.1016/j.apgeog.2008.02.007

Vojtek M, Vojteková J. 2019. Flood susceptibility mapping on a national scale in Slovakia using the analytical hierarchy process. Water. 11(2):364.

Wang D, Zhang Y, Zhao Y. 2017. LightGBM: an effective miRNA classification method in breast cancer patients. In: [place unknown]; p. 7–11.

Wang Y, Hong H, Chen W, Li S, Panahi M, Khosravi K, Shirzadi A, Shahabi H, Panahi S, Costache R. 2019. Flood susceptibility mapping in Dingnan County (China) using adaptive neuro-fuzzy inference system with biogeography based optimization and imperialistic competitive algorithm. Journal of environmental management. 247:712–729.

Wilson JP, Gallant JC. 2000. Terrain analysis: principles and applications. [place unknown]: John Wiley & Sons.

Xu Y, Dai Y, Dong ZY, Zhang R, Meng K. 2013. Extreme learning machine-based predictor for real-time frequency stability assessment of electric power systems. Neural Computing and Applications. 22(3):501–508.

Yamazaki D, Ikeshima D, Tawatari R, Yamaguchi T, O'Loughlin F, Neal JC, Sampson CC, Kanae S, Bates PD. 2017. A high-accuracy map of global terrain elevations. Geophysical Research Letters. 44(11):5844–5853.

Yariyan P, Janizadeh S, Van Phong T, Nguyen HD, Costache R, Van Le H, Pham BT, Pradhan B, Tiefenbacher JP. 2020. Improvement of best first decision trees using bagging and dagging ensembles for flood probability mapping. Water Resources Management. 34(9):3037–3053.

Ye B, Liu B, Tian Y, Wan L. 2020. A methodology for predicting aggregate flight departure delays in airports based on supervised learning. Sustainability. 12(7):2749.

Young RA, Mutchler CK. 1969. Soil movement on irregular slopes. Water Resources Research. 5(5):1084–1089.

Youssef AM, Hegab MA. 2019. Flood-hazard assessment modeling using multicriteria analysis and GIS: a case study—Ras Gharib area, Egypt. In: Spatial modeling in GIS and R for earth and environmental sciences. [place unknown]: Elsevier; p. 229–257.

Youssef AM, Pradhan B, Sefry SA. 2016. Flash flood susceptibility assessment in Jeddah city (Kingdom of Saudi Arabia) using bivariate and multivariate statistical models. Environmental Earth Sciences. 75(1):12.

Zhang J, Fogelman-Soulié F. 2018. KKbox's music recommendation challenge solution with feature engineering. In: [place unknown].

Zhang X, Aguilar E, Sensoy S, Melkonyan H, Tagiyeva U, Ahmed N, Kutaladze N, Rahimzadeh F, Taghipour A, Hantosh T. 2005. Trends in Middle East climate extreme indices from 1950 to 2003. Journal of Geophysical Research: Atmospheres. 110(D22).

Zhang Y, Zhao Z, Zheng J. 2020. CatBoost: A new approach for estimating daily reference crop evapotranspiration in arid and semi-arid regions of Northern China. Journal of Hydrology. 588:125087.

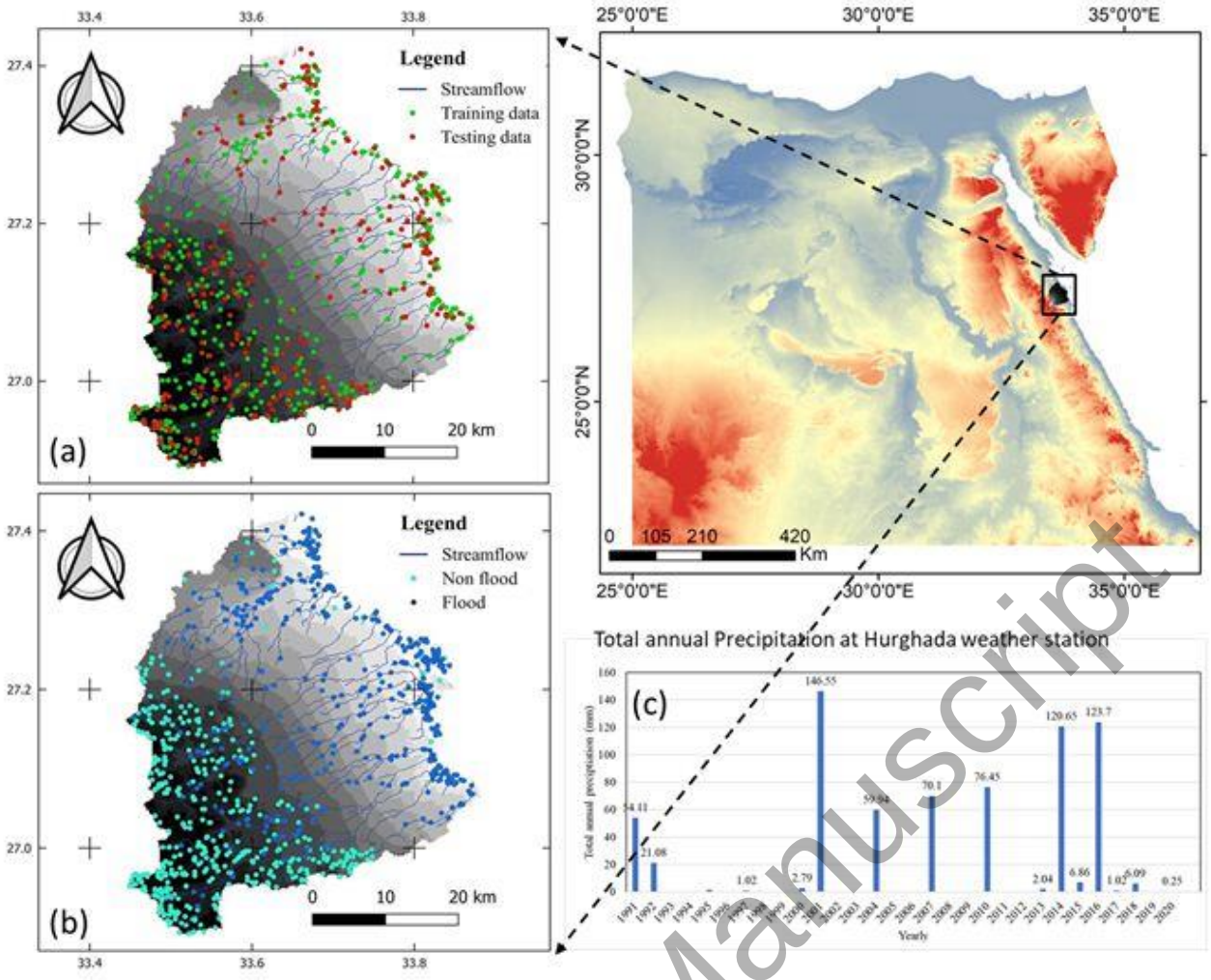

Figure 1. Map of the study area. a) Flood inventory map for the training and validation datasets. (b) Flooded and nonflooded locations. (c) Total annual precipitation at Hurghada weather station.

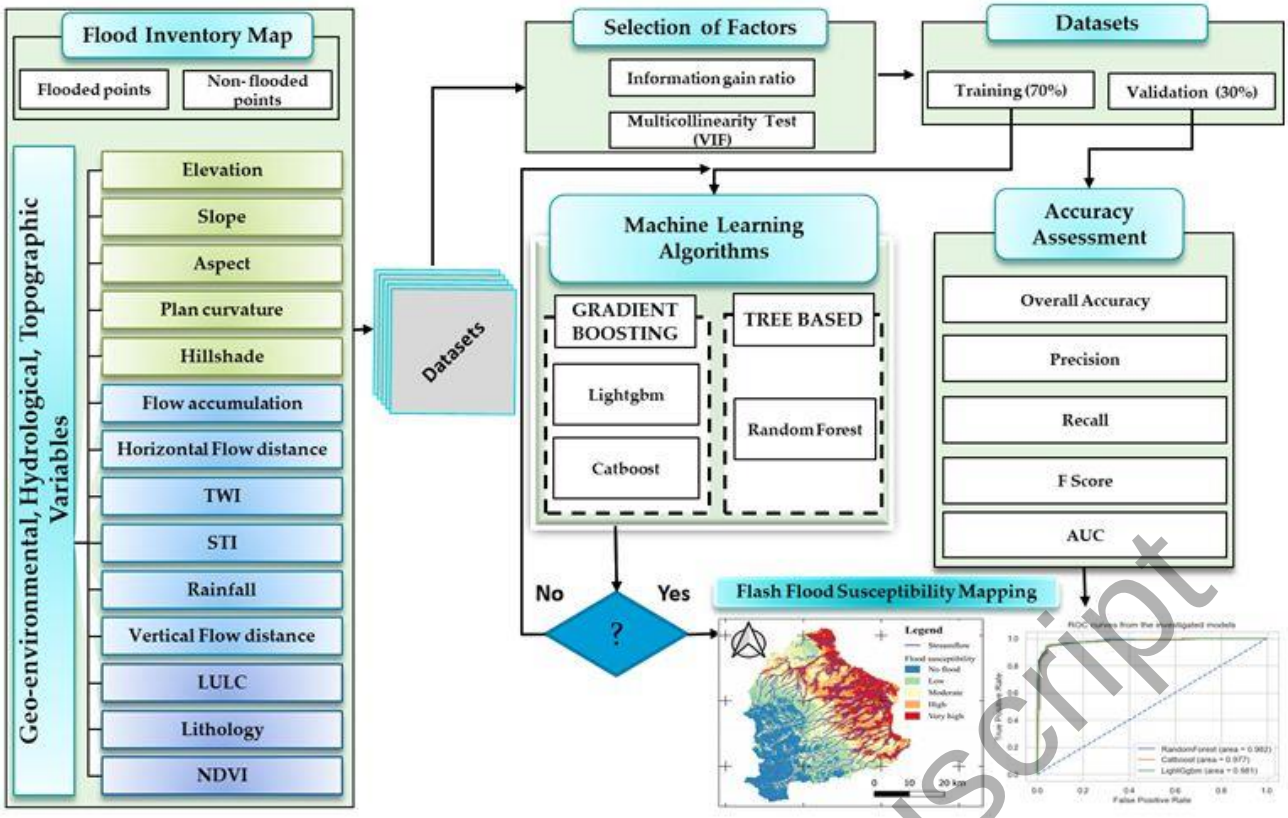

Figure 2. Methodological flow chart for FFSM.

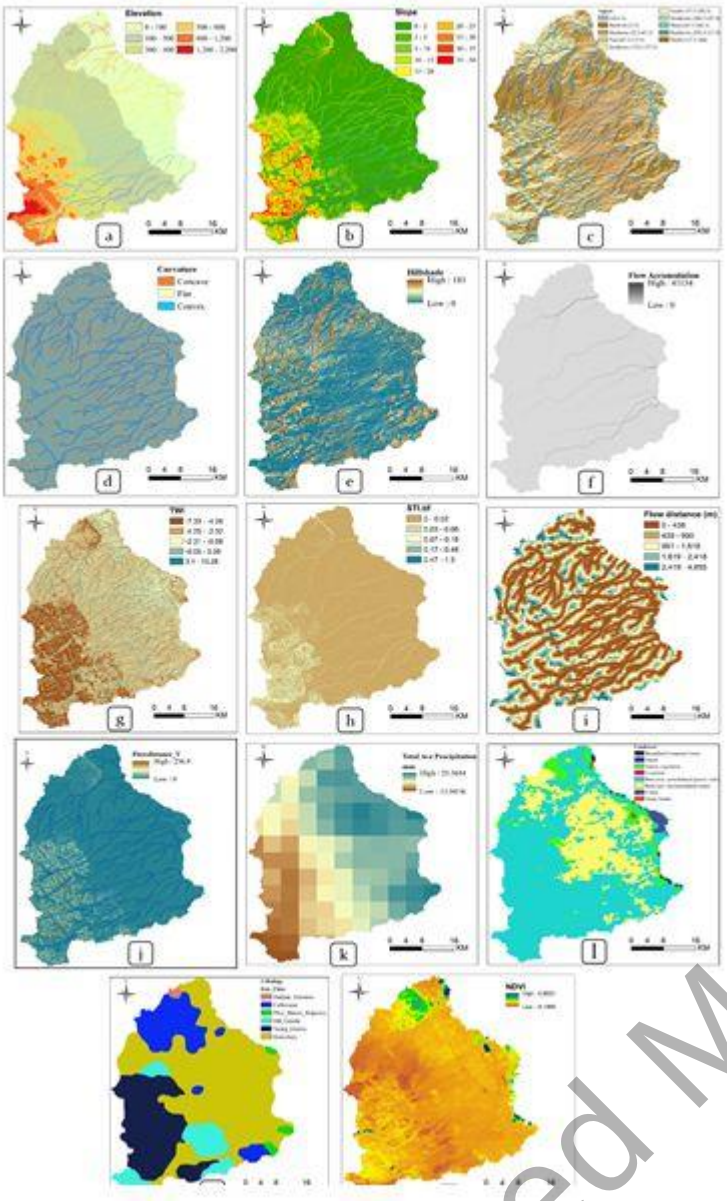

Figure 3. Controlling factors that influence flash floods: (a) elevation, (b) slope, (c) aspect, (d) plan curvature, (e) hillshade, (f) flow accumulation, (g) the TWI, (h) the STI, (c) horizontal flow distance, (i) vertical flow distance, (j) rainfall, (k) flow distance, (l) LU/land cover, (m) lithology and (n) the NDVI.

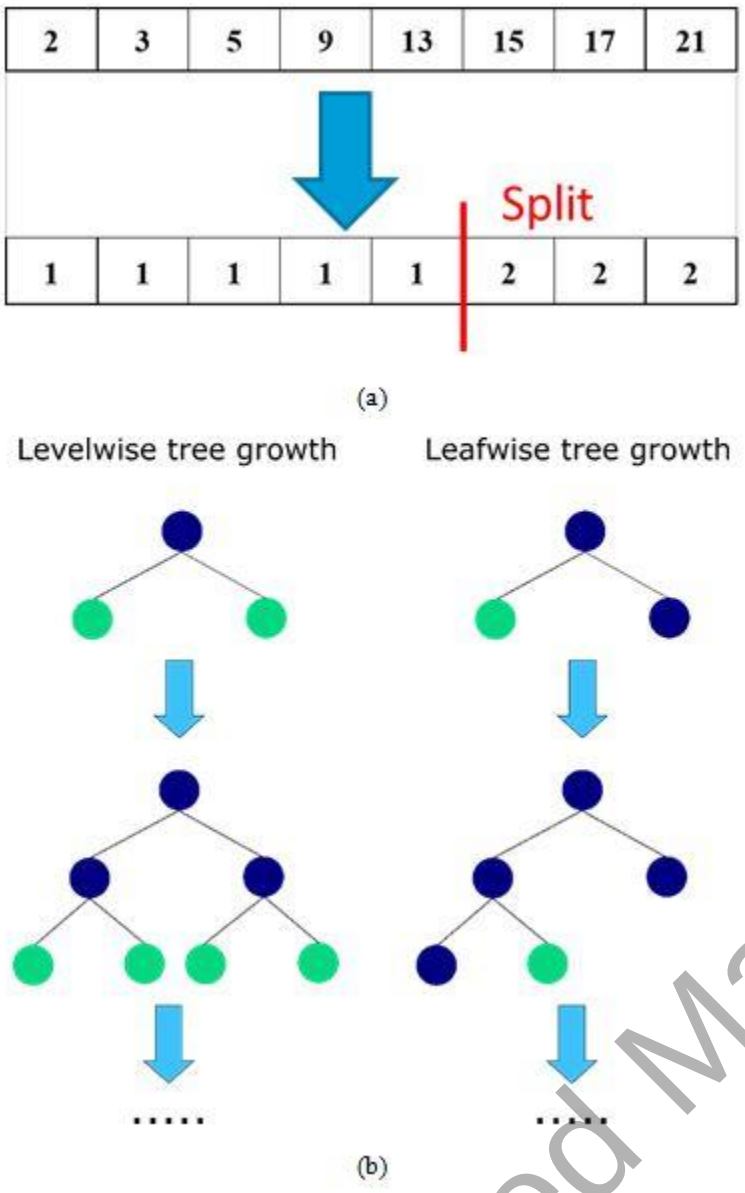

Figure 4. a) Histogram-based algorithm scheme and b) levelwise and leafwise tree growth.

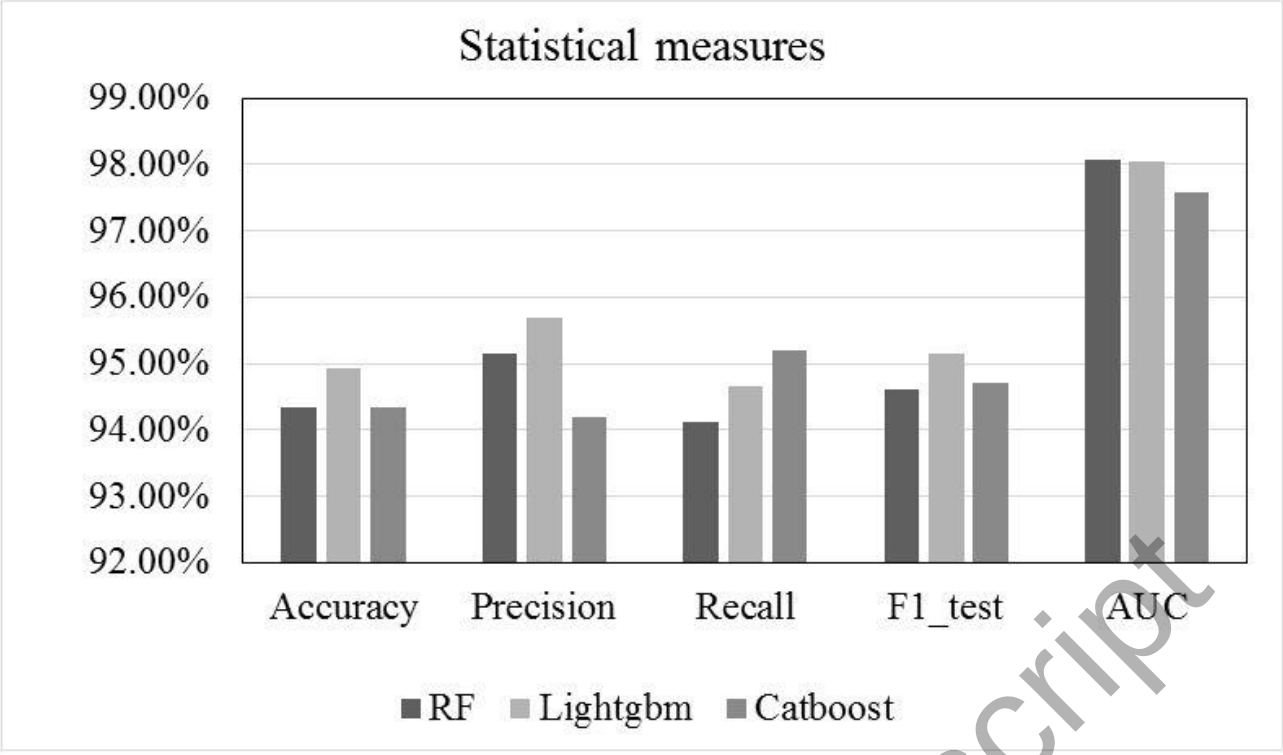

Figure 5. Statistical measures used in the model performance evaluation (RF, LightGBM, and CatBoost).

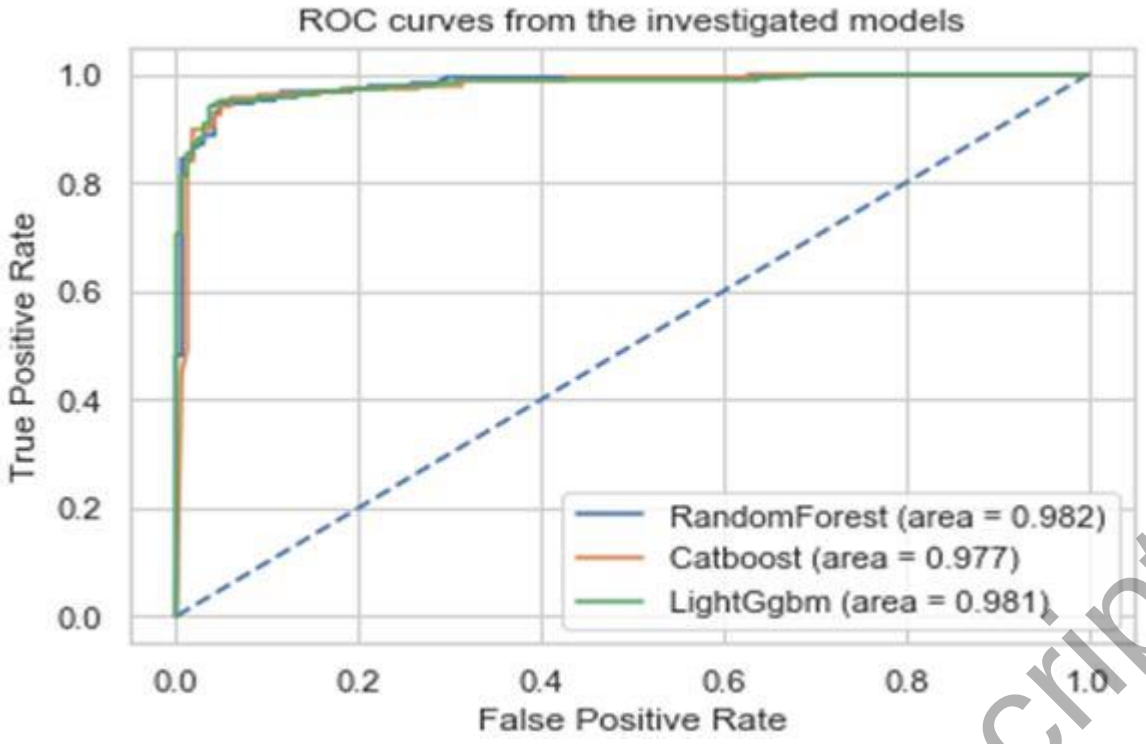

Figure 6. Areas under the ROCs for all models used.

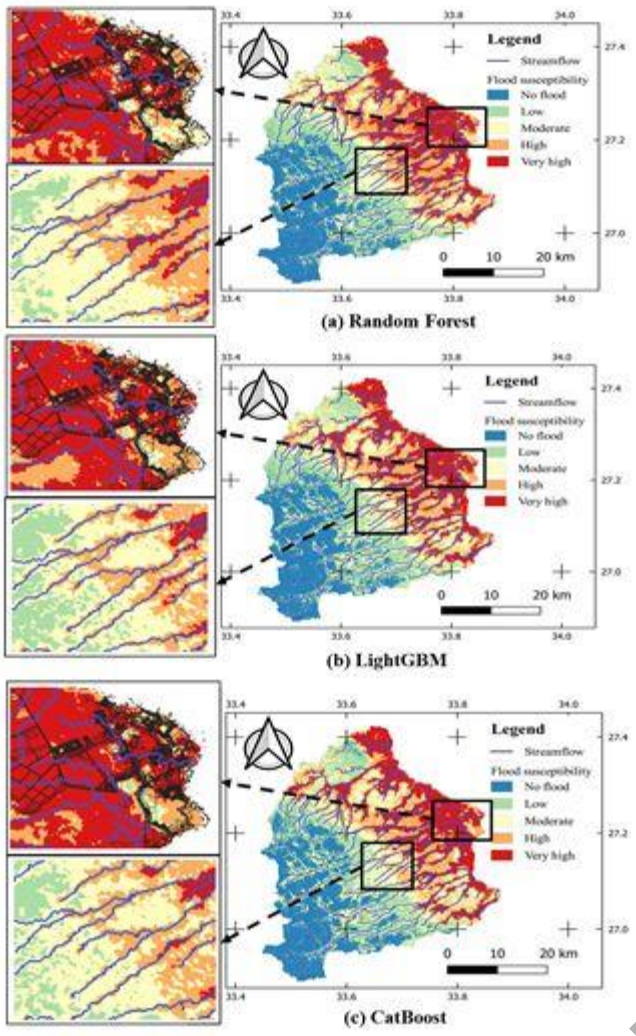

Figure 7. Flood susceptibility maps based on the (1) RF, (2) LightGBM and (3) CatBoost models.

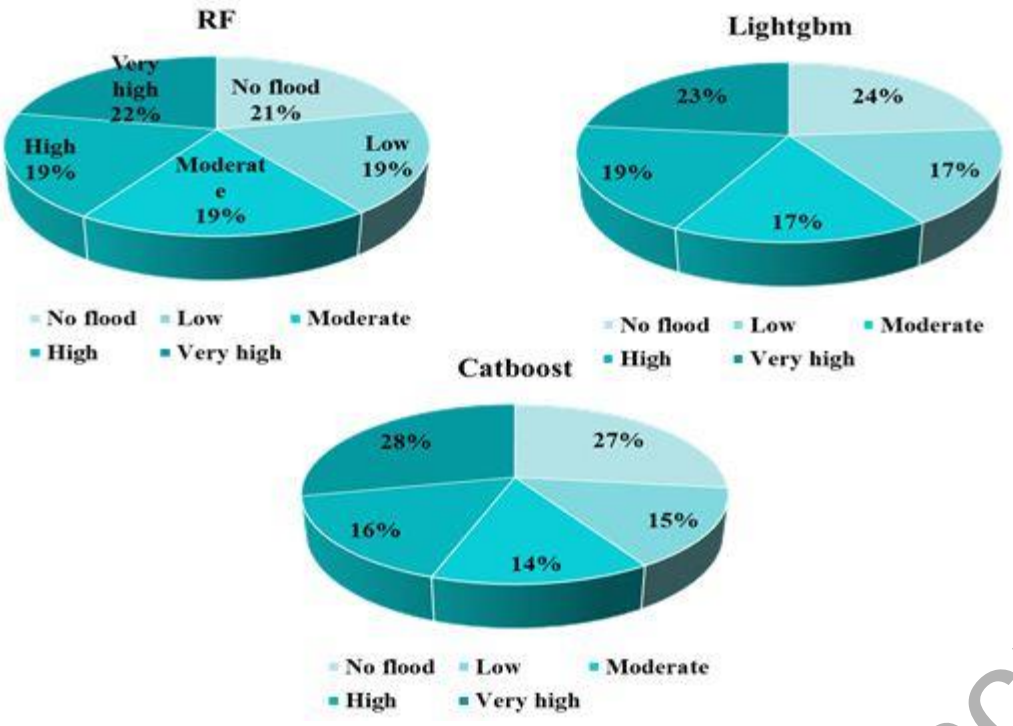

Figure 8. Percentage of the study area associated with each flood susceptibility class based on the RF, LightGBM and CatBoost models.

Table 1. The optimal hyperparameters for Random Forest, Lightgbm and Catboost models.

Methods	Hyperparameters	Grid search values	Selected value
RF	Max depth	[2:2:40]	18
	Number of trees	[100:100:2000]	1100
LightGBM	Learning rate	[0.01:0.01:0.1]	0.08
	Max depth	[2:2:40]	40
	Number of leaves	[20:20:300]	220
	Min data	[5:5:100]	5
CatBoost	Learning rate	[0.01:0.01:0.1]	0.01
	Max depth	[2:2:40]	4
	Leaf estimation iterations	[1:1:10]	10
	l2-leaf reg.	Log[10(-21), 10(-8)]	Log(10(-21))

Appendix A

Fig. A.1. Flash flood disaster effects in urban areas in the city of Hurghada (a-e) and in highway areas (f) (Jihad Alansary 2014; Abdulwahab Aboualnaga 2014; Mohamed Soliman 2015; Courtesy Abdelhameed 2016).

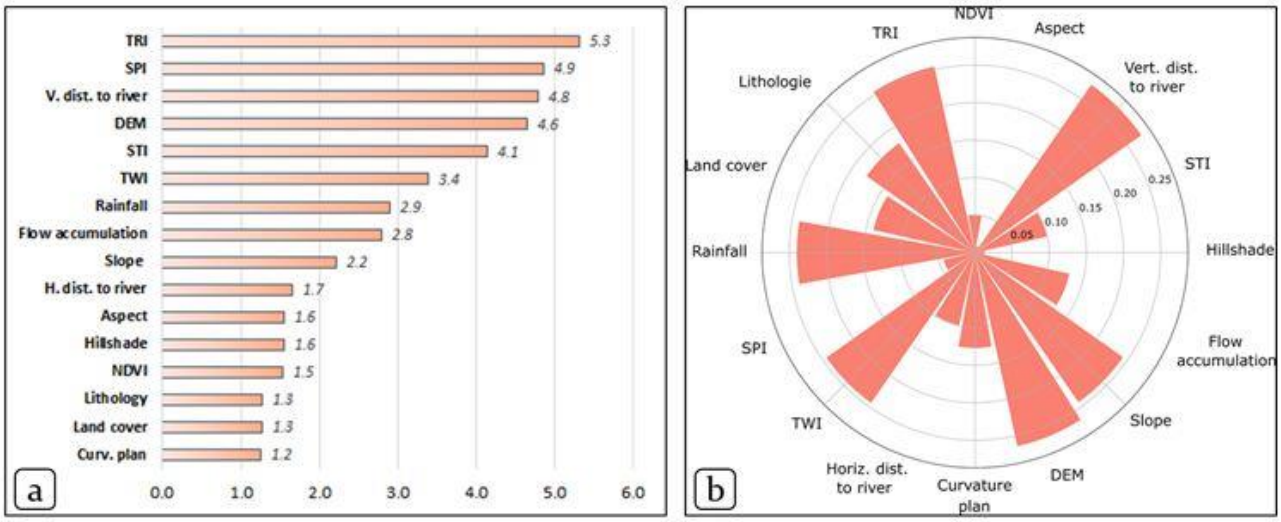

Fig. A.2. Multicollinearity analysis of influential factors: (a) VIF and (b) IGR for flood susceptibility.

Table A.1. Spearman correlation coefficients for FFSM.

	Aspect	*V. Dist. To river*	*H. Dist. To river*	*Hillshade*	*Flow Accum.*	*Slope*	*DEM*	*Curv. plan.*	*SPI*	*STI*	*TRI*	*TWI*	*Land cover*	*Lithology*	*Rainfall*	*NDVI*
Aspect	1.00															
V. Dist. To river	-0.03	1.00														
H. Dist. To river	-0.09	0.90	1.00													
Hillshade	0.04	0.02	-0.02	1.00												
Flow Accum.	0.04	-0.52	-0.53	-0.05	1.00											
Slope	0.12	0.34	0.09	0.05	-0.10	1.000										
DEM	0.02	0.33	0.12	0.01	0.10	0.54	1.000									
Curv. plan.	0.01	0.22	0.15	0.01	-0.35	-0.03	-0.16	1.00								
SPI	0.02	-0.27	-0.28	-0.01	0.62	0.13	0.25	-0.67	1.000							
STI	0.09	-0.05	-0.21	0.03	0.54	0.56	0.48	-0.48	0.83	1.000						
TRI	0.13	0.30	0.05	0.06	-0.01	0.95	0.62	-0.09	0.22	0.63	1.000					
TWI	-0.08	-0.50	-0.32	-0.07	0.60	-0.53	-0.17	-0.55	0.69	0.28	-0.43	1.000				
Land cover	-0.17	0.08	0.12	-0.03	-0.05	-0.12	-0.06	0.02	-0.04	-0.11	-0.12	0.06	1.00			
Lithology	-0.07	-0.09	0.02	-0.01	-0.05	-0.34	-0.40	0.08	-0.11	-0.28	-0.42	0.14	0.08	1.00		

Rainfall	-0.02	-0.15	0.01	0.00	-0.11	-0.42	-0.82	0.17	-0.23	-0.41	-0.49	0.11	0.14	0.31	1.00	
NDVI	0.07	-0.07	-0.03	0.01	-0.04	-0.07	-0.34	0.08	-0.03	-0.07	-0.08	0.00	-0.05	-0.03	0.33	1.00